OBSERVATION OF SEASONAL VARIATION AND CHEMICAL ANALYSIS OF PM_{10}

By

Mussarat Nosheen

00000114296

Master of Science

in

Environmental Science

Institute of Environmental Sciences and Engineering (IESE)

School of Civil and Environmental Engineering (SCEE)

National University of Sciences and Technology (NUST)

Islamabad, Pakistan

2018

OBSERVATION OF SEASONAL VARIATION AND CHEMICAL ANALYSIS OF PM_{10}

A thesis submitted in partial fulfillment of the requirements for the degree of

Master of Science in **Environmental Science**

By

Mussarat Nosheen

00000114296

Institute of Environmental Sciences and Engineering (IESE)

School of Civil and Environmental Engineering (SCEE)

National University of Sciences and Technology (NUST)

Islamabad, Pakistan

2018

CERTIFICATE

It is certified that the contents and forms of the thesis entitled

OBSERVATION OF SEASONAL VARIATION AND CHEMICAL ANALYSIS OF PM_{10}

Submitted by

Mussarat Nosheen

Has been found satisfactory for the requirements of the degree of Master of Science in Environmental Science

Supervisor: _____

Dr. M. Fahim Khokhar

Professor

IESE, SCEE, NUST

Member: _____

Dr. Zeeshan Ali Khan

Assistant Professor

IESE, SCEE, NUST

Member: _____

Dr. Sofia Baig

Assistant Professor

IESE, SCEE, NUST

THESIS ACCEPTANCE CERTIFICATE

Certified that final copy of MS/MPhil Thesis written by **Ms. Mussarat Nosheen (Registration # NUST201463472MSCEE65214F)** of IESE (SCEE) has been vetted by undersigned, found complete in all respects as per NUST Statues/Regulations, is free of plagiarism, errors, and mistakes and is accepted as partial fulfillment for award of MS/MPhil degree. It is further certified that necessary amendments as pointed out by GEC members of the scholar have also been incorporated in the said thesis.

Supervisor: _____

Dr. Muhammad Fahim Khokhar

Dated: _____

Head of Department: _____

Dated: _____

Principal: _____

Dated: _____

This thesis is dedicated to my Parents and My Sister Beenish Khan

for their endless support, care and encouragement that gave me strength, and

determination to accomplish my goals

ACKNOWLEGMENTS

Thanks to the Lord of the Worlds, the Beholder, **Almighty Allah**, the Most Compassionate, Merciful, and Gracious, who blessed me with health, wisdom, affectionate family, talented teachers, helping friends, resources and opportunities, enabling me to complete my thesis in the best possible manner.

This work would not have been possible without the support and guidance of many people. Firstly, I offer my sincerest thanks to my supervisor **Dr. Muhammad Fahim Khokhar** for his support, valuable assistance and suggestions. I would like to extend my deepest thanks to the GEC members, **Dr. Zeeshan Ali Khan**, and **Dr. Sofia Baig** for their endless support and help. Their interest, suggestions and valuable input has been vital in completing this work.

I would like to extend my gratitude for **Pakistan Institute of Nuclear Science and Technology** for facilitating the sample analysis and providing the necessary support and guidance. I would also like to acknowledge the US-Pakistan Center for Advanced Studies in Energy (USPCAS-E) for sharing their meteorological data for the study.

I express my greatest appreciation for my **fellows** for their immense support, good wishes, and encouragement. My deepest gratitude to my friend **Mehwish Haq** Nawaz for supporting me. My sincere thanks to the entire **C-CARGO** family for offering vital support in fulfilling the requirements of this study. I am thoroughly indebted to the valuable suggestions and help offered by **Naila Zeb**, **Tehreem Mustansar** and **Asadullah Shoaib**. I am also grateful to the staff and students of **IESE, NUST** for their help and support.

I have great pleasure to express my utmost gratitude to my loving, helping, and supportive **parents,** my **(late) Aunt,** for her unconditional love and unflinching support **and** to my **siblings**, particularly my sister **Beenish Khan** for supporting me in my decision to pursue Masters' and standing by my side. I owe all of my achievements to my family. They have always been a source of inspiration to keep me determined.

Mussarat Nosheen

TABLE OF CONTENTS

LIST OF TABLES

Chapter 4

LIST OF FIGURES

Chapter 3

Chapter 4

LIST OF ABBREVIATIONS

Chapter 1

Clean Air Act	CAA
National Ambient Air Quality Standards	NAAQS
National Environmental Quality Standards	NEQS
Suspended Particulate Matter	SPM

Particulate Matter ≤ 10 μm	PM_{10}
Particulate Matter ≤ 2.5 μm	$PM_{2.5}$
World Health Organization	WHO
International Agency for Research on Cancer	IARC
Particulate Matter	PM
Volatile Organic Carbons	VOCs
Polycyclic Aromatic Hydrocarbons	PAHs
Black Carbon	BC
Aerosol Optical Depth	AOD
Receptor Model	RM
Synchrotron Radiation X-ray Fluorescence	SR-XRF
Micro-Orifice Uniform Deposit Impactor	MOUDI
Polytetrafluoroethylene	PTFE
Methane Sulphonic Acid	MSA
Radio Frequency	RF

Initial Radiation Zone	IRZ
Normal Analytical Zone	NAZ
Photo-Multiplier Tube	PMT
Charge-Injection Device	CID
Charge-Coupled Device	CCD
Photodiode Array	PDA
Moderate Resolution Imaging Spectroradiometer	MODIS
National Aeronautics and Space Administration	NASA
Earth Observing System	EOS
Hierarchical Data Format	HDF
Environment for Visualizing Images	Envi
Interactive Data Language	IDL
Hybrid Single Particle Integrated Trajectory	HYSPLIT
U.S.-Pakistan Center for Advanced Studies in Energy, NUST	UP-CASEN

Standard Temperature and Pressure	STP
Relative Humidity	RH
Wind Direction Index	WDI
Air Resources Laboratory	ARL
Real-time Environmental Applications and Display sYstem	READY
Azad Jammu & Kashmir	AJK
Khyber Pakhtoonkhwa	KPK
Gilgit Baltistan	GB
Enrichment Factor	EF

ABSTRACT

The federal capital of Pakistan, Islamabad, is a planned city. Situated within the Potohar Plateau, it is located in the country's northwest. Compared to other major cities, it is relatively clean. It is considered as much cleaner compared to the other major cities of the country. But the influx from other cities, continuous and rapid development as well as influence from Rawalpindi, Islamabad's twin city; is deteriorating its air quality at a faster rate. Very few studies have been conducted to account for the air quality situation with primary focus on the industrial sectors and to monitor the background aerosol pollution in Islamabad. To fill the gap, 24- hourly PM_{10} samples were run once or twice a month for one year within the premises of National University of Science and Technology, Islamabad. The highest PM_{10} concentration was observed for December 2015, with 295.17 $\mu g/m^3$, while the lowest was observed for the month of July with 8.37 $\mu g/m^3$. The influence of meteorological conditions such as temperature, wind speed, wind direction, relative humidity as well as u and v wind vectors was explored using statistical tests. Only relative humidity (RH) had a significant correlation with particulate matter. Whereas, regression analysis showed that temperature, pressure, Wind Direction Index (WDI) and u wind tend to explain 62% variance in the PM_{10} concentration. The samples were analyzed to determine the presence and concentrations of heavy metals (Cd, Cr, Cu, Fe, Ni, Pb, Zn), using ICP-OES. Of these metals, only copper and nickel had siginificant correlation coefficients with meteorological parameters. Copper had a positive correlation with relative humidity. Whereas, nickel had negative correlation with WDI, and positive correlation with RH and v wind. The order of concentrations followed Zn > Fe > Pb > Cu > Cd > Cr and N. To understand the origins of these heavy metals enrichment factor (EF) was calculated, determining whether they have a crustal or anthropogenic source, by taking Fe as the reference metal. Compared to the local soil, Cd showed the highest enrichment followed by Zn, Cu and Pb, while Cr and Ni showed no enrichment.

Chapter 1

Introduction

1.1 Background

The Clean Air Act (CAA) passed in the United States of America in 1970, required the establishment of **primary** (to protect the health of population, including the sensitive population) and **secondary** (to protect public welfare) *National Ambient Air Quality Standards* (NAAQS) (NAAQS Table, 2016). This lead the USEPA to identify six frequently occurring air pollutants, referred to as the 'Criteria Pollutants'. One of these pollutant is particulate matter, regulated as PM_{10} and $PM_{2.5}$ (Criteria Pollutants, 2018**).**

In Pakistan, the Pakistan Environmental Protection Act passed in 1997 serves as the basic foundation of Pakistan's Environmental Law. The *National Environmental Quality Standards* (NEQS) were approved for the implementation of this law (Environmental Law in Pakistan, 2016). The NEQS include 24 hourly and annual standards for particulate matter, regulating particulate matter as suspended particulate matter (SPM), particulate matter ≤ 10 μm (PM_{10}) and particulate matter ≤ 2.5 μm ($PM_{2.5}$) (NEQS, 2010).

World Health Organization's (WHO) International Agency for Research on Cancer (IARC) in its 2013 assessment declared outdoor air pollution, including particulate matter (PM) as carcinogenic to humans. Air pollution and PM cause an increase in the occurrence of lung cancer (Ambient (outdoor) Air, 2018 and IARC, 2013). Outdoor ambient air pollution was accounted for 4.2 million premature deaths/year in 2016. The deaths were caused by exposure to $PM_{2.5}$, causing diseases such as respiratory and cardiovascular diseases, as well as cancer. 91% of these premature deaths occur in low-medium income countries, mostly affecting countries in South-East Asia and

the Western Pacific. Though some of these deaths may be attributed to more than one risk factors (Ambient (outdoor) Air, 2018).

PM's health risks roots from its small size. PM_{10} when inhaled may enter the lungs and get deposited there. However, $PM_{2.5}$ is even more dangerous, since it goes further and enters the blood circulation (Ambient (outdoor) Air, 2018). PM_{10} has been associated with the occurrence as well as severity of disease. Higher concentrations of either PM size fractions cause lower pulmonary functionality as well as higher respiratory issues among those at risk, such as asthmatics. PM concentrations even within the permissible limit have been linked to hospital admission due to respiratory problems.

Besides size, the chemical composition as well as shape of the PM affect its toxicity. Combining these factors with the mass concentration influence the health effects of these PM. It is made of a complicated combination of both solid and liquid particles, both organic and inorganic in nature, hanging in the air. The main constituents include like nitrates, sulfates, sodium chloride, ammonia, black carbon, water and mineral dust (Ambient (outdoor) Air, 2018). Usually the coarse fraction of PM (PM_{10}) contains chemical elements from natural sources whereas the fine fraction ($PM_{2.5}$) usually consists of elements from anthropogenic sources (López et al., 2011).

Elemental composition of the PM is important to find for the characterization of aerosol samples. Even though the elements do not form bulk of mass concentration of PM, they provide valuable input into the source apportionment studies. Extending the studies to assess the spatial and temporal estimates of aerosols allow for more thorough source assessments. It also helps with identifying the role of meteorology, since the aerosol concentrations are dependent on the local meteorological conditions. For example, Córdoba records higher PM in winter than in other

seasons, due to lower precipitation and continuous thermal inversion conditions (López et al., 2011).

1.2 Definition and Size Distribution

Suspended particulate matter (SPM) is defined as a complicated, multi-phase system comprising of low vapor pressure liquid and solid particles hanging in the air, their aerodynamic particle sizes ranging between < 0.01 and ≥ 100 μm (Compendium Method IO-2.1, 1999). The particles are different in terms of size, shape, number, origin, source, solubility, surface area and chemical composition (Kim, 2017). New research regarding the transfer and modification of particles indicate that the atmospheric particles exist in predominantly two different modes; namely the fine (<2.5 μm) and coarse (2.5-10.0 μm) mode particles (Compendium Method IO-2.1, 1999). Studying the size distribution and chemical constituents of PM gives the data required to identify the source as well as the likely formation processes it might have gone through (Simonetti et al., 2018).

Defined only on the basis of their size and ability to be airborne, PM are inherently diverse in nature. The particles are mainly comprised of soot, ash, pollen, smoke, dirt, dust, metals and even pollen. And depending on their source of origin they may have a variety of physical as well as chemical characteristics (Bansah et al., 2016). PM's dimensional distribution is known to be closely dependent on its sources of emission and helps identify the consequent health impacts. Coarse PM is known to usually come from physical breaking and crushing procedures or re-suspension (Simonetti et al., 2018). Therefore, normally they are made up of finely divided minerals like the oxides of calcium, potassium, aluminum, silicon and iron. Coarse particles of soil or dust mostly result from entrainment by the motion of air or from other mechanical action within their area (Compendium Method IO-2.1, 1999). Bio-aerosols also constitute part of coarse PM

(Simonetti et al., 2018). Whereas, the fine PM is mainly released as a result of fuel and biomass burning; also formed by the formation of secondary aerosols as the precursor gases interact.

Studying the dimensional distribution of PM offers information regarding dust aging. Dust aging itself, is dependent over distance between the originating and sampling sites, as well as the prevalent climatic conditions. As the particles gain stability in the atmosphere, smaller particles increase their size via condensation. And larger ones minimize their size via wear and tear (Simonetti et al., 2018).

1.3 Formation

The atmosphere has different kinds of particles. Those directly emitted in the atmosphere are called primary PM, whereas those formed as a result of gas to particle conversion processes are called secondary particles. Primary particles consist of soot, mineral dust, salt particles as well as pollen and spores. Secondary particles are made up of gases like organic compounds, nitrates and sulfates.

Formation of secondary particles follows three steps as the particle increase in size or transform. The first step in the formation of particulate matter is nucleation. Depending on the concentration of gases and atmospheric conditions like temperature and humidity, the gas phase may transform into liquid or solid phase via chemical reaction or condensation. Thus forming the first nuclei or particle. The second step involves the condensation of gases, thus generating the primary aerosols. The third and final step is called coagulation. Here the aerosols formed in the previous step begin to cluster together via turbulence, Brownian motion and interaction between particles. Therefore, forming secondary particles (Falcon-Rodriguez, 2016).

Coarse particles are formed by mechanical processes like grinding and wearing. Therefore, it is made up of finely split minerals like oxide of iron, calcium, potassium, silicon and aluminum.

Other coarse particles consist of dust or soil; they become part of PM via physical activity or air motion (Compendium Method IO-2.1, 1999). Whereas, the fine particles start off as gases, later increasing in size via processes such as combustion, transformation or condensation. Finally reaching a relatively stable size in the atmosphere. Since fine PM initiate as gases, these consist of metals, organic aerosols, combustion products and inorganic ions (sulfates, nitrates and ammonia). Coarse particles tend to have a smaller retention time in the atmosphere than the fine particles due to their larger size (Compendium Method IO-2.1, 1999).

1.4 Sources

1.4.1 Natural and Anthropogenic Sources

PM are released in the air from different natural and anthropogenic sources (Taiwoet al., 2014). Once released, these particles become airborne and are enabled to cover long distances by virtue of their small size. Concentration of PM at a particular place may vary on a daily and even hourly basis because of instability in the atmosphere or wind speed or direction variation (Bansah et al., 2016).

PM from natural sources is released by biomass combustion, volcanic activity, sea spray, soil and rock debris, biogenic release and as products of reactions between gases released from natural sources. Wind-blown dust is another source, but 25% of emitted dust particles are of anthropogenic origin. Anthropogenic sources of dust PM include emissions from mining or construction activities (Bansah et al., 2016). Anthropogenic source is susceptible to a lot of variation and remains a matter of concern for the governments, agencies working for environment, researchers and the general population due to its considerable contribution towards air pollution (Bansah et al., 2016).

PM from anthropogenic sources are released from sources like agriculture, industry, transportation, biomass burning, mining, fossil fuel combustion, construction, brake and tire wear and pavement erosion via traffic (Lindbom et al., 2006, Taiwo et al., 2014 and Bansah et al., 2016). The major anthropogenic contribution in terms of trace elements usually comes from exhaust emissions from mobile or industrial sources as well as fugitive emissions from sources like building construction, industry, agricultural activities, traffic re-suspension and erosion from storage piles and uncovered surfaces. For example; pavement wear and tear can release metals PM containing metals such as sodium, calcium, potassium, cadmium, aluminum and silicon (Lindbom et al., 2006). Whereas, break and tire wear release PM with metals like copper, lead, zinc and antimony (Bansah et al., 2016).

1.4.2 Primary and Secondary Particulate Matter

Another classification on the basis of source includes the primary and secondary particulate matter. The particles directly emitted in the atmosphere are known as primary, whereas those formed as a result of chemical reactions between the precursors are referred to as the secondary PM (Kim et al., 2017). Including both natural and anthropogenic PM, the primary particles come from sources like volcanic eruptions, biogenic material like pollen, sea salt, suspended road dust from traffic, biomass burning and mineral dust, released either as solids or liquids (Bansah et al., 2016).

Secondary PM are formed as a result of the gas to particle conversion in the air. And are an outcome of the atmospheric aging of the particles suspended in the air. These are formed via the interaction of precursors like sulfur dioxide, nitrogen dioxide and volatile organic compounds. The process occurs through the physical and chemical interactions between the particles, leading to their transformation. As the particles transform, they go through changes in their size and

structure via gas uptake, coagulation, restructuration as well as the chemical reactions. Such transformational phenomenon takes place in the clouds. The contribution of secondary particles to the total PM is well documented, where sources with anthropogenic origins tend to have a greater percentage than the natural ones in the atmosphere (Bansah et al., 2016).

1.5 Composition

The chemical composition of particulate matter is diverse and consists of organic compounds, water soluble ions, organic compounds (Taiwo et al., 2014), metals, polycyclic aromatic hydrocarbons, inorganic ions, biological components and the particle-bound water, inorganic ions, metals, particle-bound water, polycyclic aromatic hydrocarbons (PAH) and biological components (Bansah et al., 2016). Main components include elemental and organic carbon, sulfates, nitrates and crustal material. Emitted from both natural and anthropogenic sources, either directly or as precursors like SO_2, NO_2 and VOCs (Bansah et al., 2016).

Each of these components has a significance and gives important information about the sources that release them. Like the water soluble ions, which make an important part of the PM mass, have a significant role in the aerosol chemistry. Nitrates and sulfates in the PM come from the oxidation of NO_x and SO_2. Magnesium, sodium and chloride constitute the major part of sea spray. Calcium is released from construction processes, emissions from steelworks and soil. Whereas, potassium's sources include soil and biomass burning. Various biological, geological as well as anthropological sources release trace metals in the air. Different sources and processes forming the PM influence the dimensional distribution of these particles. Each of the chemical component comes with a distinguishing dimensional distribution, depending on its source (Taiwo et al., 2014).

1.6 Health Effects

PM related health effects have been observed at very low level exposure to PM, with no proof of a safe level beyond which no adverse health effects could occur. It could be attributed to the complex, microscopic structure of PM, deriving from a variety of natural and anthropogenic sources (Almeida et al., 2015).

PM size distribution is important to determine the health effects of PM. As their size determines their penetrability in the respiratory tract and the eventual deleterious effects (Simonetti et al., 2018). PM penetrate the respiratory pathway depending on the size distribution via inhalation. $PM_{2.5}$ is much smaller in size, thus enters the alveoli, eventually entering the systemic circulation. This leads to respiratory health problems like asthma, chronic obstructive pulmonary disease and even lung cancer. PM causes toxicity via mechanisms such as inflammation, genotoxic and epigenetic variations and oxidative stress (Kim et al., 2017).

Generally, fine PM is linked to higher incidence of lung cancer, cardiac arrhythmias and higher death due to cardiovascular diseases. Coarse PM on the other hand, has been held responsible for cardiopulmonary morbidity and respiratory diseases. Though some researchers were unable to find a direct link between coarse PM and health effects (Simonetti et al., 2018). PM exposure leads to increased morbidity and mortality, atherosclerosis, as well as higher hospital admission as a result of cardiovascular and respiratory problems (Almeida et al., 2015 and Bansah et al., 2016).

Healthy people are susceptible to non-permanent symptoms when exposed to high PM levels. But children, older people and those with lung or heart issues are more vulnerable to the adverse effects of PM pollution (US EPA, 2015). Research in epidemiology has linked the short and long term $PM_{2.5}$ exposures to higher mortality, morbidity as well as emergency hospital

admissions for diabetes, neurological disorders, cerebrovascular, cardiovascular and ischemic heart problems (Javed et al., 2015 and Bari and Kindzierski, 2016). The short-term effects of exposure to PM are primarily caused by particulate released by diesel (Bansah et al., 2016). Whereas, the link between these health issues and PM is more pronounced for $PM_{2.5}$ than for larger sized particles, due to its ability to reach the alveoli (Javed et al., 2015). On a global scale, nearly 3% cardiopulmonary and 5% lung cancer related deaths are accounted for by particulate matter (Almeida et al., 2015).

PM is also found to trigger atherosclerosis, causing sever birth difficulties. Children, the elderly and those suffering from chronic respiratory diseases are more prone to adverse effects of PM exposure. Children exposed to PM tend to have problems in lung development, leading eventually to retarded lung growth as well as functionality. Kids with asthma are also found to experience aggravated asthmatic condition (Bansah et al., 2016). International Agency for Research on Cancer (IARC), WHO's agency dedicated to cancer, categorized PM as a human carcinogen. The World Bank (2006) estimated that in Pakistan PM related annual health burden constitutes 1% of the gross domestic product. And found that 22,000 premature deaths among adults and 700 among the kids were caused by PM pollution (Javed et al., 2015).

1.7 Importance of Chemical Composition

There is not enough data to determine different effects of particles with a varying chemical composition or coming from different sources. But sufficient evidence exists about the importance of identifying particle chemical composition, besides particle number and mass concentration to better assess health risks associated with PM (Bari and Kindzierski, 2016). PM and the associated chemical species not only serve as a beneficial air quality index, but also as indirect information about the presence of other primary and secondary pollutants. The chemical composition has been

studied extensively to identify the potential sources and formation processes behind the PM. Other reasons include its importance in determining the impacts of chemical composition over visibility, climate change and its associated health risks. Therefore, PM mass concentration studies and the identification of their toxic components is a prerequisite for epidemiological studies and air quality management (Javed et al., 2015).

Some of the trace elements and their compounds (e.g., arsenic, cadmium, chromium, cobalt, nickel, lead, mercury, manganese, antimony, selenium) are considered as toxic (arsenic, lead, mercury, cadmium, nickel). Literature indicates that elements derived from the crust (e.g., silicon, aluminum, calcium, iron) dominate $PM_{10-2.5}$. These tend to be potentially less toxic than the combustion-derived trace elements (e.g., lead, arsenic chromium, nickel, zinc, cadmium and selenium) abundant in $PM_{2.5}$. Thus establishing the notion that the source, composition and small sized particles are significant in toxicity (Bari and Kindzierski, 2016).

1.8 Effect on Atmosphere

PM can cause air pollution, smog, numerous impacts over cloud microphysics as well as direct and indirect effects on global carbon, sulfur, nitrogen and hydrological cycles (Khokar et al., 2016). One of the most important components in the atmosphere, PM form the seed for cloud or fog formation, causing precipitation. Different pollutants both absorb and scatter radiation. An increase in these pollutants' concentration in the air can have harmful consequences. Such as affecting the cloud formation, reduction in the clouds' precipitation rate as well as visibility (Bansah et al., 2016 and Bulbul et al., 2018)

Different parts of the country undergo severe haze and fog from December – February, causing serious social as well as economic consequences, specifically the disturbance of road and air traffic (Bulbul et al., 2017). High pollution, particularly elevated PM coming from various

sources, is a major cause behind the persistent fog each winter over Pakistan (Alam et al., 2016). Both PM_{10} and $PM_{2.5}$ have been reported to have double their average concentrations during severe fog (Bulbul et al., 2017). The elevated concentration is characterized by a low activation super saturation point (Alam et al., 2016). While the lower temperature and higher humidity conditions of the winter season tends to enhance the fog (Bulbul et al., 2017).

PM pollution is a threat to the peaceful existence of the living organisms and their environments. The effects of PM on the terrestrial and aquatic ecosystems has been the subject of attention recently. Chief environmental impacts of PM have been reportedly caused by poor visibility, acid deposition and ozone. They also minimize both the utility and aesthetic value of the building material (such as the stone, cement, metals and paint) as well as cultural monuments via processes like soiling and corrosion. The building materials undergo this damage as the surface particles catalyze the degradation, when it comes in contact with heat, air and moisture. The corrosion process is further enhanced beyond the regular rate when the PM serve as the nucleation site for the acidic gases such as SO_2 and NO_2, resulting in the formation of acidic PM. The acidic PM tend to minimize the life of paints via discoloration, soiling and loss of gloss and thickness. Acidic deposition can have negative effects on aquatic and terrestrial ecosystems such as effects on rivers, streams, lakes, soil, aquatic organisms and forests (Bansah et al., 2016).

A serious concern about PM pollution is related to reduction in visibility. Fine PM are well known for visibility reduction by absorption and scattering of the visible light. Sulfate has been found to be a major element in PM to be affecting the scattering of light as well as visibility. The mean contribution from various elements in the PM towards visibility reduction was found to be 16% for nitrate, 40% for sulfate and 22% each for the elemental and organic carbon (Bansah et al., 2016).

1.9 Effects on Energy Budget

PM play an important role in earth's energy balance (Alam et al., 2016). Dust particles suspended in the air tend to change the pathway of short and long wave radiation via scattering and absorption in the air, warming the atmosphere as a result of absorption (Khokhar et al., 2016). Elevated PM concentrations have a substantial influence people, plants and animals as well as on climate (Alam et al., 2016).

The degree of direct and indirect effect of aerosols depends on the amount of hygroscopic as well as strong absorbing material in the PM (Salam et al., 2003). Different types of PM have diverse properties and thus a variety of effects on the extent of aerosol radiative forcing (Khokahr et al., 2016). Indo-Asian PM affect radiative forcing via a complicated set of both heating and cooling processes, where clouds and black carbon turn out to be playing the most significant roles (Salam et al., 2003). Black carbon is established as an absorbing aerosol facilitating global warming. The extent of the impact of BC varies across the world (Khokahr et al., 2016).

1.10 Present Study

The present study presents the result of an intermittent year-long sampling of PM_{10} (inhalable size particulate) over IESE, NUST Islamabad. The samples were analyzed for the presence of selected heavy metals and the both the datasets were statistically tested for the influence of meteorology on their respective concentrations. Satellite based monitoring of the aerosols was carried out by measuring Aerosol Optical Depth (AOD) levels, which serve as surrogate for aerosol measurements, for each sampling day.

1.11 Justification of the Study

With the increasing economic and industrial development, masses change their lifestyles. This in turn enhances the urbanization process even more, adding the pressure on fossil fuels for

energy and for an incessant supply of contemporary facilities for consumers. This cause an array of both organic and inorganic chemicals to be released in the environment. Causing environmental degradation, toxicity as well as incidence of diseases (Waheed at l., 2012).

Asia has undergone enormous economic development, particularly in the previous decade, besides going through expansive urbanization, motorization and energy consumption on a large scale. PM is present everywhere in the air and remains a vital indicator of air quality (Siddique et al., 2012). The extensive developmental activities have caused air pollution, where PM pollution particularly poses a significant risk to the environment and population's health (Bulbul et al., 2017). These pollutants have proved to be very problematic for countries undergoing development such as Pakistan, India and China, causing increasing concerns about the airborne PM at all levels (Shahid et al., 2018).

Unforeseen and massive urbanization as well as ground and air traffic has led to crowded cities. Making conditions suitable for smog formation, which itself results from the presence of PM and soot. Smog can corrode metal structures as well as building materials. PM from the anthropogenic sources on the other hand, is a precursor for climate change (Waheed et al., 2012). PM also poses a huge health burden as well, WHO attributed 22,000 premature adult deaths and 700 children's deaths in Pakistan to PM pollution (Javed et al., 2015). In Pakistan regular dry spells and calm winds encourage the suspension of dust and pollution from anthropogenic sources. The suspension is either removed as a result of a strong dust storm in dry conditions or helps form clouds of fine dust (haze), possibly reducing visibility (Waheed et al., 2012).

Islamabad, with its large scale roads and well thought-out structures is a clean city compared to large cities like Karachi, Lahore or even Islamabad (Bulbul et al., 2017). But the inflow of people in search of economic opportunities, its geographic location, swell in the number

of industries and vehicles, as well as brick kilns located in its suburbs using high in sulfur coal have contributed to the deterioration of air quality in Islamabad deteriorating (Siddique et al., 2012 and Waheed et al., 2012). And its ongoing development, including extension of the road networks and construction of new buildings and housing schemes to accommodate the people coming in Waheed et al., 2012 and Bulbul et al, 2017) is also likely to enhance the air pollution.

Therefore, it is imperative to monitor the air quality as the city dynamics change and it undergoes developmental and climate changes. Particulate Matter is one of the criteria pollutants, and much of its hazardous and toxic attributes as well as health risks come from its constituents. It is important to identify the most crucial information, to eventually facilitate a preventive and remedial action plan.

1.12 Benefits of the Study

Islamabad used to be a pristine land and still remains much cleaner compared to major cities of the country. But its air quality has suffered in recent years. Several studies indicate that on many occasions pollutants exceeded the National Environmental Quality Standards. There is a huge increase in industrial and construction activities; including housing, road infrastructure and commercial mega malls cropping up throughout the city. All these activities have consequences which need to be assessed to identify processes and ways to avoid or minimize the damage. The study may also set a precedent, where similar and new more innovative researches might help explain the air quality issues of Islamabad. It could add value to the existing knowledge and may facilitate policy and decision makers to abate air pollution in Islamabad.

1.13 Objectives of the Study

1. To collect ground based data for PM_{10} and satellite observation

2. To investigate the selected heavy metals in PM_{10} samples collected during selected period

3. To investigate the relationships between PM_{10}, Heavy Metals and meteorological variables

Chapter 1 introduces the topic, reasons behind carrying out the research, the aims and objective of the study as well as the expected outcomes. Chapter 2 presents the literature reviewed during the course of this research, covering various international and national works, as well as those conducted within Islamabad. Chapter 3 describes the study area, the methodology adopted to carry out the study, as well as the instrumentation and working principles of the instruments utilized. Chapter 4 discusses the results in detail. Whereas Chapter 5 is the final chapter containing the conclusions and recommendations.

Chapter 2

Literature Review

2.1 PM Size Distribution

Generally, PM is classified into three broad groups; ultrafine (<0.1 μm), fine (0-2.5 μm) and coarse (2.5 - 10 μm) mode particles. Ultrafine and fine PM are usually attributed to processes involving high temperature, like industrial activities, biomass burning, coal and oil combustion, exhaust from vehicles as well as the chemical transformations that take place in the atmosphere. Coarse particles on the other hand are linked to processes involving wear and tear. Examples include brake and tire wear, erosion from crustal material, re-suspended road and soil dust, sea spray and volcanic eruptions (Taiwo et al., 2014).

Taiwo et al. (2014) studied size fractionated components of PM in an industrial coastal town and an urban background site in the **United Kingdom**. And noticed considerable differences in the dominant size range at either sites. Prominence within particular size ranges and exhibition of particular patterns helped identify the possible sources contributing to the observed results. At both sites, mass concentrations, sodium and potassium ions, iron, copper and barium exhibited two modes of peaks, typically at 0.5–0.6 μm and at 2–6 μm. Fine PM concentrations were slightly higher at the urban background site, and the industrial site showed higher coarse PM concentration due to the to higher marine aerosols (chlorine, sodium and magnesium ions) and metallic elements, most prominently iron and manganese.

Iron and manganese show an enhanced coarse mode within the same size range at the industrial site, depicting links with a similar steelworks source. Sulfate and ammonium (SO_4^{2-} and NH_4^+) were more abundant at the urban location, linked to the regional transport of secondary

ammonium sulfate. Nitrate ion (NO_3^-) was found noticeably coarse as compared to ammonia (NH_3) at both sites, though relatively a little fine than Cl^- and Na^+. Literature shows this to be a marker size distribution for aged marine aerosol.

Overall the concentrations were higher at the urban site, due to the east-west secondary sulfate and nitrate gradient observed across UK. K^+ showed similar modes at both the sites though the concentrations were found to be higher at the industrial site. Fine K could mainly be contributed by wood smoke, whereas the coarse particles could be contributed in part by the marine aerosol as well as by emissions from steelworks. Coarse Ca^{2+} concentrations were very high at the industrial site, probably the result of steelworks processes and stockpiles. Manganese and Iron were considerably higher in the coarse range at the industrial site due to a common steelworks source. Aluminum and Vanadium concentrations were found in higher concentrations at the urban site. The likely sources of Al could be soil or road dust, whereas fuel oil could be contributing to V concentrations. Cu, Sb and Ba concentrations were higher at the urban site, their mode at 3 μm size distribution being characteristic of the break wear emissions. Zn, Pb, Sb and Cu showed a considerable peak from 0.4-0.5 μm, linked to high temperature procedures. Except Zn, the remaining were found to be more prominent at the urban site. Zn showed modes at 0.4 μm and 2 μm, more prominently at the industrial site, particularly in the coarse range and has been associated with the steelworks emissions.

PM samples were studied in **Istanbul**, Turkey (Şahin et al., 2016) at five locations, including four urban and one rural site, to depict variability in source. Here the PM showed three modes of distribution; two each in each of the fine and coarse PM and one for most elements in either fine or coarse PM. Trace elements like V, Ni, Pb and Cd dominated the fine mode PM (<1 μm), whereas Mn, Co, Fe, Ca Mg and K were prominent in the coarse PM (>3 μm). Most peaks

for Zn, Se and Sn were observed in the fine mode (< 1 μm) at the site called **Avcilar**. These metals exhibited high concentrations in the summer samples, which was attributed to the industrial activity around the sampling site. V and Pb were also primarily dominating in the fine fraction (< 2.6 μm), considered to be pollutants of anthropogenic origin via the fossil fuel (oil) use for heating purposes. At the Avcilar sampling site, V and Pb were dominant likely due to the power plant located in the western side of site, employing fossil fuels to generate energy.

Among all the metals of soil origin (Mn, Fe, Ca and Mg) 65-80% were observed in the coarse fraction. Whereas, metals like Pb (82%), Cd (53%), Se, V and Sn (48%) primarily dominated the fine mode (<2.5 μm) in the first urban site. The concentrations were even higher during the heating season. A similar trend of higher concentrations during the heating season was observed for other sites as well. Mg (55%) also had a considerable presence among the fine mode PM. On the contrary; the coarse mode metals (Mn, Cu, Zn, Ba and Ca) showed a decrease in concentration during the heating period.

2.2 PM and Meteorology

Air quality of a city is mainly affected by two things, its geography and atmospheric conditions of the region (Şahin et al., 2016). The harmful effects of pollution on the atmosphere depend not only on the size of the emitted pollutant but also on the weather conditions. Although weather normally helps to disperse the pollutants, it may also worsen the air pollution or provide the conditions for the formation of even more harmful chemicals. PM has been found to travel thousands of kilometers to reach it destination. Weather parameters primarily influencing the PM concentration include air temperature, humidity, precipitation, wind speed and direction as well as solar radiation. Precipitation is a vital means of clearing the atmosphere, where it collides with the PM, washing them down. Therefore, the presence of a long lasting precipitation, be it moderate or

intense is understandably important as a mechanical clearing process, having extended positive implications (Czarnecka et al., 2007).

Patterns in a data which are either controlled or depend upon season of the year is referred to as seasonality. It may depend upon parameters such as temperature, wind direction and other meteorological parameters. Emission interruptions, such as planned shutdowns that occur each year in the same season may also contribute to effects of seasonality (Bari and Kindzierski, 2016). Li et al. (2017), studied the temporal and spatial variation of PM (PM_{10} and $PM_{2.5}$) and its relationship with meteorology in a city in northeast China. And observed several seasonal or annual patterns in terms of PM concentrations and ratios as well as the role meteorology played in these patterns. They found that the both the PM_{10} and $PM_{2.5}$ monthly concentrations were higher during winter and autumn season but lower during spring and summer. Even the monthly ratios between the coarse and fine fraction PM showed higher values in winter and autumn but they were found to be lowest during spring, indicating a higher coarse fraction due to dust activity.

Seasonal and annual variations were observed between the PM concentrations and meteorological parameters. Both the size fractions showed a negative correlation with visibility. The correlations were positive for temperature, pressure, and relative humidity, but negative for wind speed for most seasons. It was because of the PM dispersion that the strong wind speeds cause, but in spring the winds favored the release of coarse dust. An inverse relationship between temperature and PM was observe. Because although higher temperature promoted photochemical processes, facilitating the transformation in the secondary particles, it facilitated an efficient vertical dispersion in seasons like autumn and winter. Whereas high pressure, combined with downdrafts restricted PM's upward movement. Therefore, causing a buildup of PM within the boundary layer. Relative humidity normally has a positive relationship with PM, where higher

relative humidity resulted in higher PM concentrations due to aerosols' hygroscopic effect. But in case of in $PM_{10;}$ it showed a negative relationship in spring and summer, because in spring the dust emissions were suppressed in the wet atmospheric conditions. Whereas, the high summer rainfall caused the wet scavenging effect (Li et al., 2017).

2.3 Source Apportionment

Source apportionment consists of local studies, which intend to identify the likely sources that contribute to ambient PM concentrations measured at representative sites. The chemical components of the measured PM depict 'chemical fingerprints', hinting at the various sectors as the likely sources the PM could be attributed to.

The source apportionment could be carried out using various methodologies such as the emissions inventories, source oriented models, and the receptor model. The last two models offer the benefit of information derived from the measurements carried out in the real world. Their limitation lies in dealing with highly reactive species. A receptor model intends to attribute the concentration of a pollutant at a particular site to its sources by solving the following equation;

$$x_{ij} = \sum_{k-1}^{p} g_{ik} f_{kj} + e_{ij}$$

where x_{ij} is the concentration of the *j*th species in the *i*th sample, g_{ik} is the contribution of kth source to *i*th sample, f_{kj} is the concentration of the *j*th species in the k_{th} source, and e_{ij} is the residual for each sample/species.

RMs typically attribute the PM concentration because of its chemical composition, including trace elements, major ions, organic markers and its carbon related fractions (Karagulian et al., 2015).

2.4 Typical Source Categories of Source Apportionment Studies

i) Traffic

It involves the emissions from different types of vehicles. Contribution from this category comes in the form of primary PM released from exhaust, the inorganic and organic gaseous precursors of secondary PM and a considerable amount of contribution from the wear and tear of tires, brake linings and clutch. Contribution from these sources gets deposited on roads and re-suspends later due to the traffic, along with read wear and crustal and mineral particles.

ii) Industry

It is more of a diverse category and includes pollution emanating from oil and coal burning in power plants, emissions from industries like pharmaceutical, metallurgic, petrochemical, ceramic and IT hardware, and from port activities. This category may sometimes overlap with traffic or combustion sources not clearly identified.

iii) Domestic fuel burning

As the name indicates, this category includes emissions from the cooking or heating sources.

iv) Natural

Natural sources contributing to PM concentration include soil dust, minerals and sea salts. Dust consists of the elements found abundantly in the earth crust and consequently in soil. And become airborne as a result of resuspension caused by winds from bare soils or fields. Though separating the resuspension from natural sources or road dust is possible using marker species, it can be challenging at times.

v) **Unspecified Sources of Human Origin**

This category lists secondary particles of human origin, whose sources could not be clearly identified. The primary particles include those produced as a result of mechanical processes, carbonaceous particles and the fly ash particles generated from the combustion of fossil fuels at very high temperatures in the power plants using coal as a fuel. The secondary particles, as the name suggests are created as a result of reaction between primary gases such as (Non-methane VOCs, NO_2, SO_2 and NH_3). Secondary particles could consist of organic or inorganic PM.

a) **Secondary Inorganic**

Inorganic sulfate PM originates from agricultural sources. The NH_3 emitted from agriculture combines with SO_2 released from power production, shipping or industry. Whereas, NH_3 combining with NO_x emitted from residential, industrial, energy production and vehicular sources, gives way to inorganic nitrate PM. Since both nitrates and sulfates have a residence time of 3-9 days in the air, the secondary inorganic PM from either could be attributed to the long range transfer of pollutants.

b) **Secondary Organic Aerosols**

The secondary organic aerosols may either be generated directly as a result of combination between primary organics from combustion of coal, biomass or wood, and other substances or generated via combination of VOCs from biogenic sources. The non-methane VOCs are a type of secondary organic aerosols emitted from sources including evaporation from solvents consumed in industry or home (degreaser, stain remover or paint), emissions from industrial processes, transportation and combustion (Karagulian et al., 2015).

2.5 Assessment Methodologies

López et al. (2011) studied coarse and fine PM in Córdoba, Argentia between July 2009 – April 2010. Samples collected in this duration were analyzed using synchrotron radiation X-ray fluorescence (SR-XRF). It is also a non-destructive technique and offers considerable information about the elemental composition of the samples. Suitable to study both the major and minor as well as trace components of the atmospheric PM, it is a significant tool in the field of atmospheric chemistry. A major advantage offered by the SR-XRF compared to the regular XRF is the considerably lower count accumulation interval per individual sample spot. A NIST certified standard, the 'SRM 2783 Air particulate on filter media' in this case was analyzed and used as reference for quantitative analysis of the samples collected. The elements unavailable in the standard were quantified using the '109498 ICP multi-element standard solution for mass spectrometry'. For the purpose, varying concentrations of the standard solution were deposited on filter support used for aerosol sample collection.

Taiwo et al. (2014) used Micro-Orifice Uniform Deposit Impactor (MOUDI) to sample particle size and assess their distribution in a coastal industrial town and an urban background site in the UK. The MOUDI offered size fractionation at cut points of 10, 5.6, 3.2, 1.8, 1.0, 0.56, 0.32 and 0.18 μm, operating at a nominal flow rate of 21.5 L/min, collecting samples on Polytetrafluoroethylene (PTFE) filters. A total of 14 samples were collected. Each for a duration of 72 hours (except one, for 32 hours). Half of the sampled filters were used for the analysis of water soluble ions (Ca^{2+}, Mg^{2+}, $NH4^{+}$, Na+, K^{+}, NO_3^{-}, SO_4^{2-}, Cl^{-}), while the remainder was used for the assessment of trace metals (Cr, Cu, Pb, V, Zn, Al, Mn, Ba, Sb and Fe).

One half of the exposed filters was used to analyze for water-soluble ions (Na+, Mg^{2+}, Ca^{2+}, K^{+}, $NH4^{+}$, Cl^{-}, NO_3^{-}, SO_4^{2-}), whereas the other half was used to assess selected trace metals

(**Al**, **V, Cr**, **Mn**, Fe, **Cu**, **Zn**, **Sb**, **Ba** and **Pb**). To analyze the ionic species, 0.3 mL propan-2-ol was used to treat the first half to wet the surface. Followed by extracting the species of interest in 7.5 ml distilled de-ionized water, subjecting it to a mechanical shaker at 240 rpm for 40 minutes. For cationic species methane sulphonic acid (MSA) was used as an eluent, whereas KOH served the purpose for anionic species for the respective instruments. The remaining half filter paper was used to extract the trace metals. For this purpose, it was heated with dilute reverse aqua regia (2.23 M HCl and 1.03 M HNO_3) using Harrison et al. (2003) method. The filter paper was heated with 2ml of the extractant in a 4ml narrow neck bottle, at a temperature pf 100°C for half an hour. After repeating the cycle, the digest was transferred to a 15 ml bottle, 10ml distilled deionized water was rinsed into it. Before being analyzed by the Inductively Coupled Plasma Mass Spectrometry.

Şahin et al. (2016) studied total suspended particulate matter, using a cascade impactor, maintaining a flow rate of 90 l/min and using an eight stage Anderson cascade impactor with size ranges >8, 8−6.5, 6.5−5.2, 5.2−3.5, 3.5−2.6, 2.6−1.7, 1.7−1, 1−0.43, and <0.43μm. The samples were collected at four urban and a rural site, using quartz filter papers with a diameter of 81 mm. A total of 80 samples were collected, between July 2008 – August 2010. The filter papers were stored in a pre-conditioned room at temperature 20 ± 1 °C, and relative humidity 50 ± 5, for 48 hours before and after the sampling. To avoid the loss of volatile constituents, the samples were stored at 4 °C. A three step decomposition method was employed for the filter analysis, using a microwave digestion equipment. The first step involved addition of HNO_3 (6 ml) and H_2O_2 (2 ml) to the filter papers and letting them decompose at 180 ° C for 40 minutes. The second step involved the addition of HCl (2 ml) to the extracted solution from the previous step. The decomposition was carried out for 35 minutes at a temperature of 175 ° C. The third and final step involved the addition of HF to the extract from the previous step and decomposition for half an hour at a temperature of

160 ° C. The filters were completely dissolved by the end of third step. After cooling down, the extract from the final step was diluted to 30 ml using deionized distilled water. The samples were then stored at – 4 ° C before getting analyzed by the graphite and flame atomic absorption spectrometry.

Chapter 3

Materials and Methods

3.1 Study Area

3.1.1 Study Site

Islamabad is the federal capital of Pakistan, located at latitude 33°49 N and longitude 72°24 E and at an elevation of 500 masl. It is a contemporary and planned city situated in the Pothohar Plateau, in the northwestern region of the country. The city spans an area of 906 km^2, and an additional 2,717 km^2 covered by Margalla Hills in the north and northeast (Shah, 2012; Waheed et al., 2012; Bulbul et al., 2016). It is located at 14 km northeast of Rawalpindi city (together, the two cities are called twin-cities). With Margalla Hills in its north and the other sides touching the plains of Punjab and water bodies (Shah, 2012). Islamabad has a typical humid subtropical climate; with five distinct seasons. These include winter (November–February), spring (March and April), summer (May and June), monsoon (July and August) and autumn (September and October) Bulbul et al., 2016). Its ambient temperature can range between -4 °C in January – 45 °C in June (Waheed et al., 2012). While the mean annual rainfall is 1143 mm (Khwaja et al., 2009).

City's urban area has been split into various zones including residential, commercial, industrial and diplomatic zones. The sectors I–9/10 and the Kahuta Triangle constitute its industrial zone and house industries like oil and ghee production, soap/chemical manufacturing, pigments, paints, ceramics, pharmaceuticals and several other small industries (Khwaja et al., 2009; Shah, 2012).

The study site is located in NUST, which covers sector H-12 in Islamabad. The particulate matter sampling was conducted over IESE roof top, located in the western side of NUST. Kashmir

Highway is located in the north-west of the building, the industrial sectors of 1-9/10 in the north-east and the twin city of Rawalpindi in the south-east.

3.1.2 Sampling Schedule

24 hourly PM_{10} samples were collected between September 2015 – September 2016. Initially it was planned to collect three samples per month. But due to problems like instrument functioning, problems with the switch board and expected rainy events there could only be one sample collected for most of the months, two samples for just few and only in the month of March three samples were collected.

3.2 Sampling Instrument

A high-volume air sampler (Wedding and Associates) was used to measure PM_{10} at the study site. It consists of;

- Protective Housing
- High-Volume Blower
- Filter Holder
- Flow Controller
- Size-Selective Inlet

3.2.1 High Volume Air Sampler

The high-volume air sampler has a compact protective outer housing. Containing the blower, powered by an electric motor, a flow

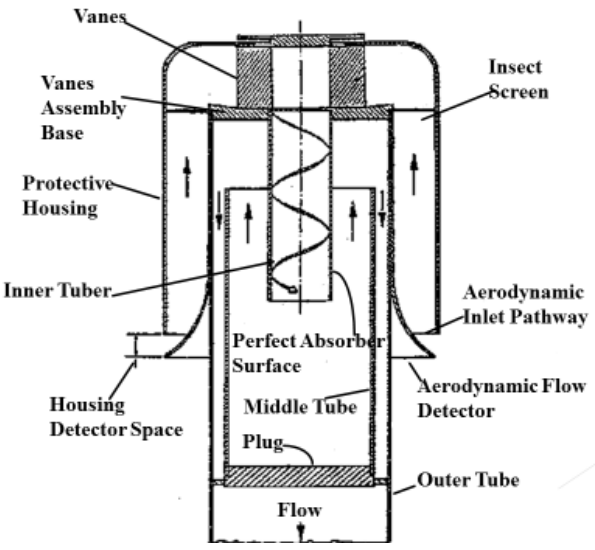

3.2.2 Size-Selective Inlet

controller, a manual timer to choose the sampler duration and a digital timer to record the sampling duration in terms of minutes. A small door allows access to the timer. At the top of the protective housing there is a filter holder, an iron casket used to hold the filter paper is fastened to the filter holder with the help of nuts. A size selective inlet is attached over the air sampler to collect particulate matter equal to or smaller than 10 micrometers. The inlet is attached at the rear end with a flexible support, allowing to turn it backwards while placing or removing the filter paper.

An electric motor powered blower draws in large volumes of air through a cyclone air inlet, which allows air to enter from all angles of approach. The air flow is regulated by a flow controller that typically maintains air flow of 1.13 m^3/m. A series of evenly spaced vanes impart an angular velocity to the air and accompanying particles. An inner tube removes the larger particles with the help of a 'perfect absorber surface' – an oil coated surface meant to remove the bounce and re-entrainment of the particle. The air now containing smaller particles enters an intermediate tube where the air trajectory is directed upwards. At this point the air stream reaches the outer tube which re-routes the air downwards once again, this time onto the filter (8" x 10"), held in place with the help of an iron mesh filter casket, to allow the PM_{10} fraction to deposit on the filter (Compendium Method IO-2.1, 1999).

3.3 Filter Material

Filters made up of quartz fiber are the most frequently used for the purpose of PM sample collection to identify the mass loading. The main features of a quartz fiber filter include: i) fiber material is made up of highly pure quartz, ii) less than 5% binder (none for the binderless kind), iii) nearly 0.5 mm thick, iv) surface free from pinholes, and v) ability to not allow more than 0.05% smoke particles to let through the filter paper at given pressure (100mm of water) and flow rate (8.53 m/min).

These filters are made of thin glass fibers, mixed with binder of organic nature and compressed into a filter using a paper machine. Their use in air sampling is increasing, likely due to higher collection efficiency. They can also resist high temperatures (<540°C). Therefore, the filter may be exposed to flash fire in certain cases, to avoid any interference from the binder during analysis that follows sampling. But the firing reduces their strength, thus requiring a backing material to be used during sampling. The non-hygroscopic nature of the filters makes them an obvious choice for high humidity areas. Since they are made of glass, they are also suitable for studies in highly corrosive environments. But filters belonging to this category are breakable and thus need to be handled with care. The high silicate content in quartz fiber filters makes them hard to ash using either chemical or heat. Thus, extraction procedures are employed to get the sample for further analysis. It is for this reason that the quartz filters exposed to flash fire constitute the majority of filters used for atmospheric sampling (Compendium Method IO-2.1, 1999).

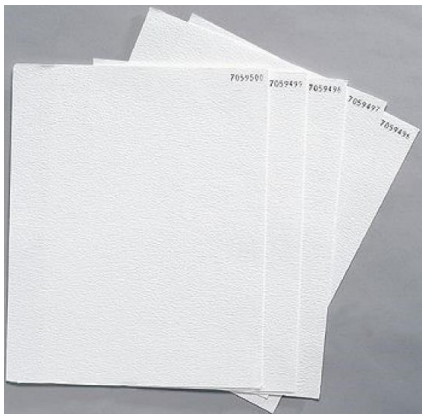

3.3.1 Quartz Filter Paper (Data Support Company)

3.4 Pre-treatment and Storage

Ambient air aerosols from the study site were collected on pre-weighed 8 x 10 inches' quartz filters (Whatman ultra-pure QMA). Particulate Matter of the size range of 10 micrometers and less (PM_{10}) were collected on a filter with an area of 8 x 10 in^2 held by a filter holder. The sampling duration was 24 hours for most samples, in a few cases the duration was smaller. Once the sampling was completed, the filters were removed with great care, folded and sealed in a polyethylene bag and stored within the laboratory environment. The filters were conditioned before and after sampling for 24 hours in the lab environment (temperature: 25°C and relative

humidity: 55%). The PM concentrations were calculated in µg/m^3 and corrected to standard temperature and pressure conditions.

3.5 Sample Calculations

The filters were conditioned in the lab environment and gravimetrically tared prior to the sampling. Post sample collection, the filters were restored to the laboratory and conditioned as previously before being weighed. The PM_{10} concentration was calculated as the mass of collected PM divided by the air volume sampled.

$$PM_{10} = \frac{W_f - W_i * 10^6}{V_{std}} \quad \text{....Eq (1)}$$

PM_{10}= concentration of particulate matter (PM^{10}), µg/ m^3.

W_i = initial weight (clean filter), g.

W_f = final weight (exposed filter), g.

V_{std} = total volume of air sampled, corrected to standard conditions (25°C and 760 mm Hg), m^3.

10^6 = to convert g to µg.

The standard volume was calculated using the formula;

$$V_{std} = (V_s)\left(\frac{P_{atm}}{P_{std}}\right)\left(\frac{T_{std}}{T_{atm}}\right) \quad \text{.... Eq (2)}$$

$$V_{std} = (V_s)\left(\frac{P_{atm}}{760mmHg}\right)\left(\frac{298K}{T_{atm}}\right)$$

$$V_{std} = (V_s)(0.39)\left(\frac{P_{atm}}{T_{atm}}\right)$$

V_{std} = volume of air sampled, corrected to EPA's standard temperature (25°C), m^3 and pressure (760 mm Hg) and

V_s = volume of air sampled at atmospheric pressure (P_{atm}) and temperature (T_{atm}), m^3.

T_{std} = EPA standard temperature (25°C), 273 + 25 = 298 K.

P_{std} = EPA standard pressure, 760 mmHg.

T_{atm} = average atmospheric temperature during sampling (°C), 273 + 25 = 298K.

P_{atm} = average atmospheric pressure during sampling, mmHg.

0.39 = 298 K/760 mm Hg (Compendium Method IO-2.4, 1999).

The samples were stored at room temperature in the laboratory till further analysis. The digestion procedure to extract metals of choice from the particulate matter was a modified version of US EPA Compendium Method IO 3.1. For the analysis, the filter papers were shredded using clean plastic scissors. The glassware was pre-washed with a 5% acidic solution, followed by a rinse each with distilled water and oven dried. A solution consisting of Nitric Acid and Hydrochloric Acid (1:3) was used. For each filter paper, 50 ml solution was poured over the shredded filter paper and heated at 130°C for half an hour. The entire procedure being carried out in a fume hood. After the heating procedure 100 ml distilled water was added to these filter papers and allowed to stand overnight. The emerging solution was then filtered using a Whatman 40 filter paper with a pore size of 150 mm. Later on, the solutions were heated without boiling to reduce volume. Once the desired volume reduction was achieved the solutions were transferred to 25ml volumetric flasks, where they were filled up to the mark with distilled water. The final extract was then transferred to plastic bottles, labelled and refrigerated until further analysis. The extract was analyzed using Inductively Coupled Plasma Optical Emission Spectrometry (ICP-OES). A brief

description of the instrument is presented in the next section. To calculate the concentration of heavy metals from the results obtained by ICP-OES analysis the following equation was used;

$$C = \frac{\left(Metal\ Conc.\frac{\mu g}{ml} x\ Final\ Extract\ Vol.\right) - F_m}{V_{std}} \ldots. \text{Eq (3)}$$

C = Metal Concentration

F_m = Average Concentration Blank Filters

V_{std} = Standard Air Volume Pulled Through Filter in standard m^3 (calculated using previous equation).

3.6 Sample Analysis

3.6.1 Inductively Coupled Plasma Optical Emission Spectrometry (ICP-OES)

3.6.1.1 Principle

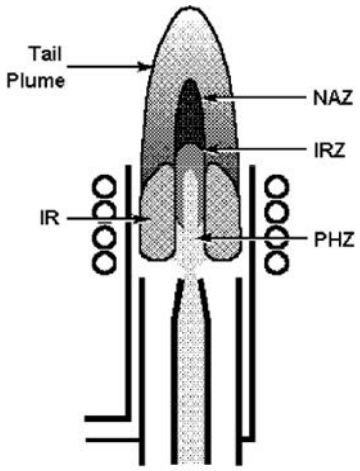

3.6.1.1 ICP Plasma Zones: IR – Induction Region, PHZ – Pre-Heating Zone, IRZ – Initial Radiation Zone, NAZ – Normal Radiation Zone

An inert gas (argon) is directed through a torch consisting of three concentric quartz (or another suitable material) tubes. While an alternate current is applied to the gas by the help of a radio frequency (RF) generator connected to the copper wire (load wire) wound around the top end of the torch. This generates both the electric and magnetic field. A spark is applied to the gas, releasing some electrons from the atoms. The magnetic field accelerates their motion, leading them to knock out more electrons from their orbits, eventually forming a combination of electrons, ions and atoms of the argon gas called the plasma; sustained through the continuous supply of RF energy. The ICP

discharge appears as a very intense, brilliant white, teardrop-shaped discharge. As the sample aerosols are injected into the plasma, they punch a hole into the center of the plasma, giving it a doughnut shape. It is in this region that the transfer of inductive energy takes place between the load coil and the plasma. The sample is supplied as a liquid, pressured by the nebulizer into a fine mist through the center of the plasma. Here the high energy plasma result in a chain of events starting with i) desolvation – removing the solvent from the aerosol and leaving microscopic salt particles, ii) vaporization – decay of the salt particles into individual gas molecules and iii) atomization – further breakdown of these molecules into atoms. The last two steps including the iv) excitation – electrons moving to a higher energy level within the shells, and v) ionization – electrons gaining enough energy to break free from the atoms (even ions go through excitation, jumping to a temporary higher energy level); of these droplets. The electrons return to their original position by emitting energy in the form of characteristic wavelength. The excitation and ionization processes occur predominantly in the initial radiation zone (IRZ) and the normal analytical zone (NAZ). The NAZ is the region of the plasma from which analyte emission is typically measured. The high temperature within the plasma renders the ICP procedure superior to other flame or furnace activation techniques. In case of ICP gas temperature in the core is nearly 6800 K, which not only helps enhance the excitation and ionization efficiencies but also reduces many of the chemical interferences found in flames and furnaces. The intensity of light emitted at each characteristic wavelength is used to determine the concentration of the element of interest. For the element detection the emitted light is separated into individual wavelengths using either a monochromator – to measure light at each individual wavelength at a time or a polychromator – to measure light at various wavelengths at the same time. Allowing a photo-multiplier tube (PMT)

or advanced detector techniques such as a charge-injection device (CID) or a charge-coupled device (CCD) to measure these.

3.6.1.2 Instrumentation

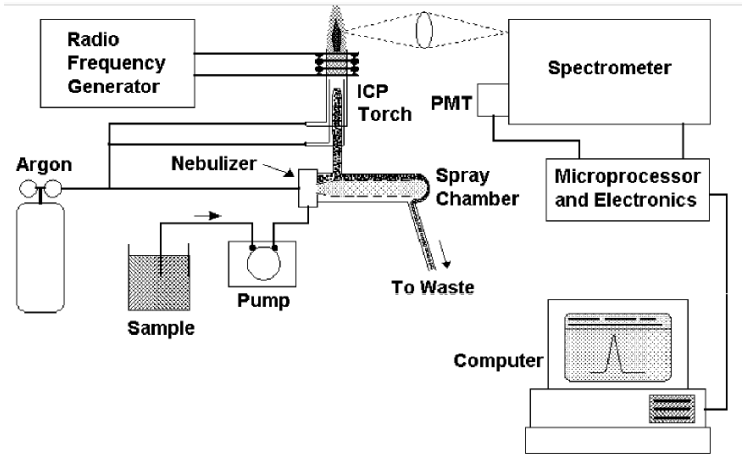

3.6.1.2 Schematic Diagram of an ICP-OES

1) Nebulizer

A nebulizer converts the liquid sample solution into an aerosol through a process called nebulization. There are two ways of doing it, either by using i) pneumatic forces or ii) ultrasonic mechanical forces. The pneumatic nebulizers use high-speed gas flows to create an aerosol. While the ultrasonic nebulization uses an oscillating piezoelectric transducer to achieve aerosol formation.

2) Peristaltic pumps

Some nebulizers are capable of drawing in the sample themselves. While others require a peristatic pump to do so. The pump employs a series of rollers to push the sample through the tubing using a process called peristalsis.

3) Spray Chamber

A spray chamber transports the sample aerosol to the torch, to be injected into the plasma. Only very small aerosols are suitable for being injected in the aerosol (≤10 mm diameter). Therefore, to inject the suitable aerosols in the plasma, a spray chamber is placed between the nebulizer and the torch. A typical nebulizer converts about 1-5% of the introduced sample to this size range. The remaining 95 - 99% of the sample is drained into a waste container.

4) Drain

It carries the excess sample from the spray chamber to the waste container. This function also allows to maintain a backpressure required to force the sample aerosol-carrying nebulizer gas flow through the torch's injector tube and into the plasma discharge.

5) Torch

The torch is responsible for the formation of plasma as well as injecting the aerosols in the plasma. It consists of three concentric tubes, each supporting a distinct gas flow; the i) outer, ii) intermediate and iii) inner gas flows. The outer gas flow, also called the plasma flow previously, spirals tangentially around the chamber with high velocity due to certain design elements. One of its functions includes keeping the quartz walls of the torch cool. The intermediate tube directs the gas flow under the plasma toroid. Thus keeping the plasma discharge away from the intermediate and injector tubes and facilitating the sample introduction into the plasma. This flow might be used to minimize the carbon formation on the tip of injector tube while analyzing an organic sample, to enhance the performance for aqueous solution or not used at all. The inner gas flow also known as the **sample or nebulizer flow** carries the sample aerosol through the central tube or injector. The small opening at the end of the injector tube imparts such high velocity to the sample aerosol, that it is able to punch a hole through the plasma.

6) Radio Frequency Generator

It is the device that provides the power to generate and sustain the plasma discharge. Powered typically between 700 – 1500 watts at frequencies ranging from 27 – 56 MHz, they transfer power to the plasma through the load coil wound around the torch at the top. The load coil consists usually of copper tubing and is cooled by either gas or water during the operation.

7) Transfer Optics

The emission radiation from the region of the plasma known as the normal analytical zone (NAZ) is sampled for the spectrometric measurement. The analytical zone may be observed either from the side (plasma in the vertical position) called the radial view or horizontally (plasma rotated to a horizontal position) called the axial view. In either cases, or a dual viewing combining both observation angles, the radiation is eventually collected by a focusing optic such as a convex lens or a concave mirror. Either modes of optics focus the image of the plasma on the entrance slit of a spectrometer which serves to disperse the wavelength.

8) Wavelength Dispersive Devices

Diffraction grating is the most common method to differentiate the emission radiation for specific elements. Lesser common options include prisms, filters and interferometers. The grating is incorporated in an instrument called spectrometer. Spectrometers for ICP-OES are optimized for 190 - 450 nm range, since most analytically useful emission lines for an ICP-OES lie within this region. A spectrometer receives polychromatic radiation (white light) and uses the diffraction grating to disperse the radiation corresponding to various wavelengths, forming the monochromatic radiation. The monochromatic radiation is then focused on one (monchromator) or more exit slits (polychromator) on the exit plane or circle, which allows the wavelengths of interest to pass while blocking the remaining. A polychromator has multiple slits and detectors, each slit corresponding to an atomic or ionic emission line for a specific element. Monochromator on the other has just one slit and detector. It processes multielement analysis by keeping either the grating or the detector fixed, while moving the other with a sufficient for a sequential analysis.

9) Detectors

Once the spectrometer successfully isolates the emission line, its intensity is measured by the detector and associated electronics. Photomultiplier tube (PMT) is the most utilized detector. It consists of a vacuum tube containing the photocathode, which releases electrons when light strikes. The released electrons are directed towards a dynode, resulting in the release of 5-6 secondary electrons per electron hitting its surface. Typically, 9-16 stages of dynodes are present in a PMT. At the end of the dynode stages, an anode collects the secondary electrons from the last dynode. Eventually the electric current estimated at the anode is taken as a relative quantification of the radiation intensity reaching the PMT. The digital information thus generated is further processed by a computer into either provide the relative emission intensity or concentration.

The advanced array detectors consist of silicon sensors. Generic solid-state detectors suitable for spectroscopic applications include i) photodiode array (PDA), ii) charge-injection device (CID) and iii) charge-coupled device (CCD). Both CCD and CID are classified as charge transfer devices (CTD), a broad class of silicon-based devices. In silicon and silicon dioxide diode, an electron is released when a photon of visible or ultraviolet wavelength hits the structure. Application of voltage across the interface leads to charge flow. CIDs employ non-destructive investigation of charge. Whereby CCDs employ a sequential destructive mode.

10) Computers and Processors

A computer control is vital to any ICP-OES instrument. Most automatic functions of the ICP-OES are controlled directly via the onboard computer. For the simplest instruments, the analysts usually use the on-board computer with the help of buttons and keypad provided on the

instrument. But all the ICP-OES instruments, are accompanied by an external computer, providing an interface for the instrument (Boss and Fredeen, 1997).

3.6.1.3 Detection Limit

The detection limits for the elements of interest for the ICP-OES used for analysis are given below.

Sr. No	Metal	LOD (µg/ml)
1	**Cd**	0.009
2	**Cr**	0.021
3	**Cu**	0.035
4	**Ni**	0.008
5	**Pb**	0.027
6	**Zn**	0.005
7	**Fe**	0.034

3.7 Satellite Data

3.7.1 Aerosol Optical Depth (MODIS /AQUA)

Besides the ground based monitoring, the remotely sensed data is turning out to be a significant addition to atmospheric monitoring, due to its huge spatial cover, regular observations and the ease with which the electronic data may be shared. Aerosol Optical Depth abbreviated as AOD, is a satellite product consisting of the measure of extinction of light as it interacts with airborne PM in the atmospheric column. It is probably the most used surrogate for PM measurement. Researchers have compared the AOD data provided by the instrument Moderate Resolution Imaging Spectroradiometer (MODIS) aboard Terra and Aqua satellites and found that they have a varying correlation coefficient (R value) between 0.12-0.9 and more for $PM_{2.5}$ and 0.2-0.6 and more for PM_{10} (Zeeshan and Oanh, 2014).

Both Aqua and Terra are NASA's satellites, where Aqua (water in Latin) is responsible for collecting huge volumes of data about earth's water cycle. It includes data about oceanic

evaporation, atmospheric water vapors, soil moisture, clouds, precipitation, snow cover on both land and sea as well as sea and land ice. Other variables estimated by the satellite include vegetation cover, radiative energy flux, aerosols, dissolved organic matter in the oceans, and air, water and land temperatures. Aqua is part of NASA's Earth Observing System (EOS) and thus was previously named EOS PM. The PM referring to it crossing the equator in the afternoon (AQUA, 2018).

As mentioned, MODIS is the main instrument on-board the Aqua and Terra satellites. Where, Aqua orbits the earth from the south to the north, crossing over the equatorial plate in the afternoon. And Terra completes its orbit from north to south, crossing over the equator in the morning. Both observe the Earth's surface in its entirety every 1-2 days, obtaining the data in the form of 36 groups of wavelengths (MODIS, NASA). It measures the parameter of interest for this study, the Aerosol Optical Depth. An integral of aerosol extinction in the atmospheric column from the surface of earth to the top of the atmosphere (Zeeshan and Onah, 2015).

3.7.2 Data Downloading and Processing

Data was downloaded from NASA Earth Observatory's website laadsweb. (https://ladsweb.modaps.eosdis.nasa.gov/search/) for the sampling days. Data was downloaded in the Hierarchical Data Format (HDF) through FileZilla, an open source software. Further processing and analysis was performed using the software Envi (Environment for Visualizing Images) and the programing language IDL (Interactive Data Language). The daily average georeferenced tiffs were added to ArcMap to create the AOD maps and extract the raster values for our area of interest (NUST).

3.7.3 Hybrid Single Particle Integrated Trajectory (HYSPLIT)

HYSPLIT model developed by the National Oceanic and Atmospheric Administration, is used to compute the air parcel trajectories. Besides these calculations, other possibilities include simulations for pollutant transport, dispersion, transformation as well as deposition. The model is most commonly used to identify the relationship between source and rector by attempting to identify the source of air masses arriving at the location of interest.

It relies on a hybrid system consisting of both a Lagrangian approach as well as the Eulerian methodology. The former involves the use of a mobile frame of reference to calculate the advection and diffusion of the air parcels, once thy leave their initial position. Whereas, the later utilizes an immobile 3-D grid as a frame of reference for the computation of pollutant air concentration (ARL, 2017).

ARL READY's online system (https://ready.arl.noaa.gov/HYSPLIT.php) allows to interactively run the model and download the results. For this study 0.5° GDAS meteorological conditions were selected, the receptor height was chosen to be 50 AGL meters, whereas the model was run for 48 hours prior to the sample collection.

3.8 Meteorological Conditions

Islamabad has a semi-arid climate. The season ranging from warm – hot & humid summers, followed by monsoon and cold winter. May and June are typically the hottest months of the year, the mean high temperature (~38 °C) recorded in June and the mean low temperature (~2 °C) observed in January. Winter season each year has a fog episode. While heavy rains and thunderstorm are observed July – September. The general temperatures in Islamabad range from cold – mild, regularly falling below 0 °C. Sparse snow falling occurs in the hills (Margalla Hills) (Hameed, 2007).

3.8.1 Meteorological Data

Since the sampling schedule avoided a potential precipitation event, weather forecast was regularly monitored from both the official website of Pakistan Meteorological Department (http://www.pmd.gov.pk/) and Accuweather (https://www.accuweather.com/en/pk/pakistan-weather). For the purpose of exploring relationship between meteorological parameters and particulate matter, meteorological data was provided by the U.S.-Pakistan Center for Advanced Studies in Energy, NUST (USPCAS-E).

3.9 Data Analysis Methodologies

All the data tabulation was carried out in MS Excel. The calculations for concentrations of particulate matter and the selected heavy metals, as well as their correction to the STP (standard temperature and pressure) conditions was also performed in the same software. The correlation analysis and regression models were run using SPSS.

Chapter 4

Results and Discussion

4.1 Meteorology

In this section the average daily meteorological conditions during the sampling period have been discussed. Meteorological conditions reported and considered for analysis are restricted to the days when PM_{10} was sampled and refers to daily averages. The parameters considered include temperature, relative humidity, wind speed/direction and atmospheric pressure. Table 4.1 shows mean values of each parameter; their respective standard deviations as well as the

	Temperature (°C)	**RH (%)**	**Wind Speed (m/s)**	**Pressure (mmHg)**
Average	23.51	54.75	1.98	708.76
SD	7.66	20.25	0.70	4.08
Max	35.17	87.55	3.13	714.68
Min	7.30	22.62	0.93	702.27

Table 4.1: Mean Values and Variations in the Meteorological Data Sep 15 – Sep 16 at NUST

maximum and minimum values. The variation in temperature during the sampling period is depicted in Figure 4.1. For ease of understanding the seasons have been broadly categorized into summer and winter. With the period from April – September considered as summer, while the months from October – March labelled as winters. Temperature starts to fall in October and continues to drop until January at the lowest daily average temperature of 7 °C, from then on it starts to increase as summers approach.

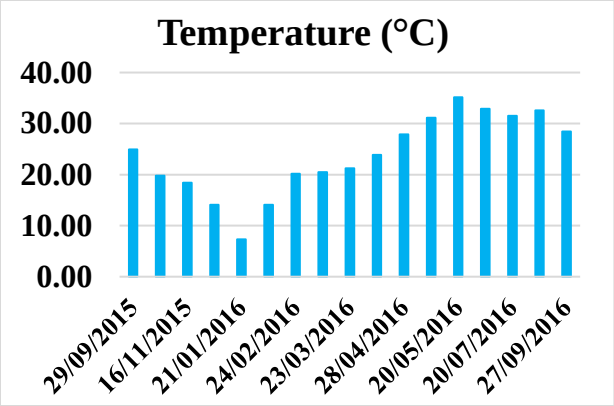

Figure 4.1: Variation in Air Temperature Sep 15 – Sep 16 at NUST

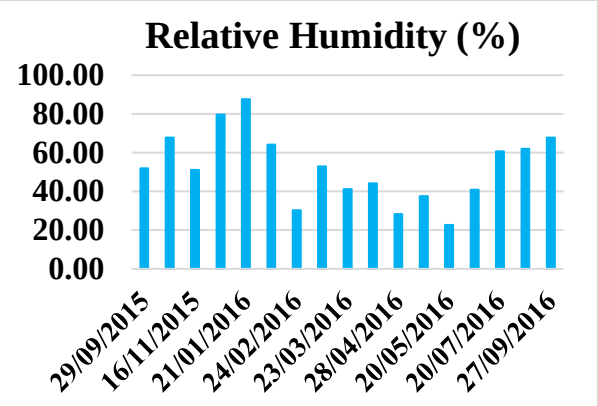

Figure 4.2: Variation in Atmospheric Pressure Sep 15 – Sep 16 at NUST

By the end of March, the temperature shoots higher (24 °C), peaking in May at 35 °C, it begins its downward trend towards September. The average daily temperature recorded in summer was recorded to be 30°C, the maximum temperature was 35 °C while the minimum was 25 °C. Winter temperature averaged at 17 °C, the maximum was 24 °C while the lowest it went to was 7 °C.

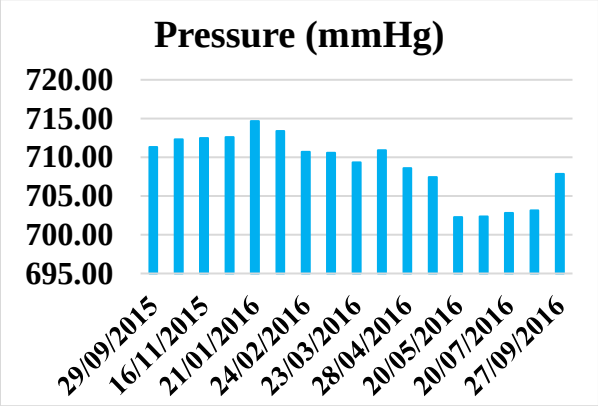

Figure 4.3: Variation in Pressure Sep 15 – Sep 16 at NUST

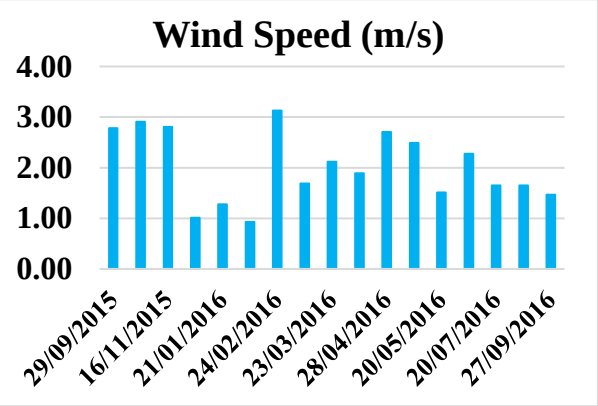

Figure 4.4: Variation in Wind Speed Sep 15 – Sep 16 at NUST

The standard deviation for both the seasons was similar (5.5 °C for summer and 5.3 °C for winter). Relative humidity depicts a directly inverse relationship with temperature, as displayed in Figure 4.2 represents the average relative humidity conditions observed during the

sampling period. The average relative humidity was recorded to be 52%. The maximum it reached was 87%, whereas the lowest was found to be 23%, and a standard deviation of 20%. Similarly, pressure also shows an opposite trend to temperature, as seen in Figure 4.3. Although the pattern is not as pronounced as of relative humidity.The average pressure was found to be 709 mmHg, the maximum value was 715 mmHg whereas the minimum was found to be 702 mmHg. The standard deviation for this variable was 4 mmHg. Figure 4.4 presents the wind speed throughout the sampling period. It shows frequent crests and troughs. The average wind speed was 2 m/s, with the maximum value as 3m/s and minimum as 1m/s, showing the least standard deviation, 0.7 m/s.

Besides these variables, three other meteorological parameters were calculated. These include the Wind Direction Index (WDI) as well as north–south (v) and east–west (u) components of the wind vector. WDI (not depicted graphically) was calculated to avoid the discontinuity of the wind directions around the North, i.e. 360°, using Eq. (1), where θ is the wind direction in radians.

$$WDI = 1 + \sin(\theta + \pi/4) \quad \text{……. Eq (1)}$$

Eq. (1) resolves the problem of variation in wind direction around 0° (or 360°) and produces similar values of WDI for these both wind angles (Zeeshan and Oanh, 2014). Whereas, u and v are the wind components. In a two-dimensional plane, a vector may be divided into component vectors **i** and **j**. Where, **i** runs parallel to the x-axis and **j** to the y-axis. In terms of wind, u wind runs parallel to the x-axis, while v wind run parallel to the y-axis.

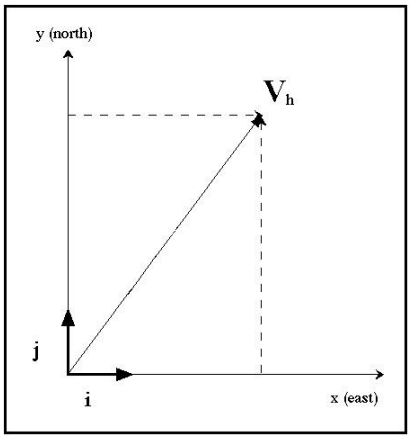

Figure 4.5: Orientation of wind vectors in a 2-D frame

Positive u wind indicates a wind from west, and **negative** means the wind is coming from the **east**. While, a **positive v** wind represents wind coming from **south** and **negative v** wind suggests its coming from **north**.

Figure 4.5 depicts the orientation of u and v vectors of wind in a two-dimensional frame. If we have the wind speed and wind direction, we can obtain the component vector winds, u and v, using Eq. 2 & 3.

u = Wind Speed X sin θ ……. Eq (2)

v = Wind Speed X cos θ ……. Eq (3) (Wind: u and v Components, 2014).

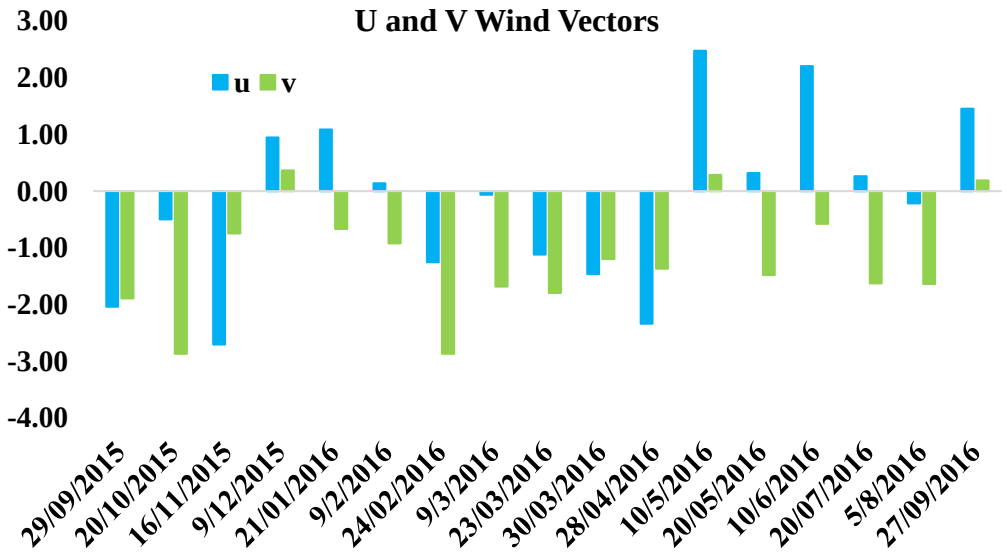

Figure 4.6: Wind Vectors Sep 15 – Sep 16 at NUST

The graphical presentation of these wind vectors can be observed in Figure 4.6. As can be seen, u wind is equally distributed between east and west.

Whereas, the overwhelming majority of v wind is coming from north.

4.2 Particulate Matter

This section discusses the gravimetric analysis of PM_{10} represented in µg/m ^{3}. Changes in the concentration of particulate matter throughout the year have been depicted in Figure 4.7. Aerosol concentrations show an upward trend, until they peak in December. The concentrations

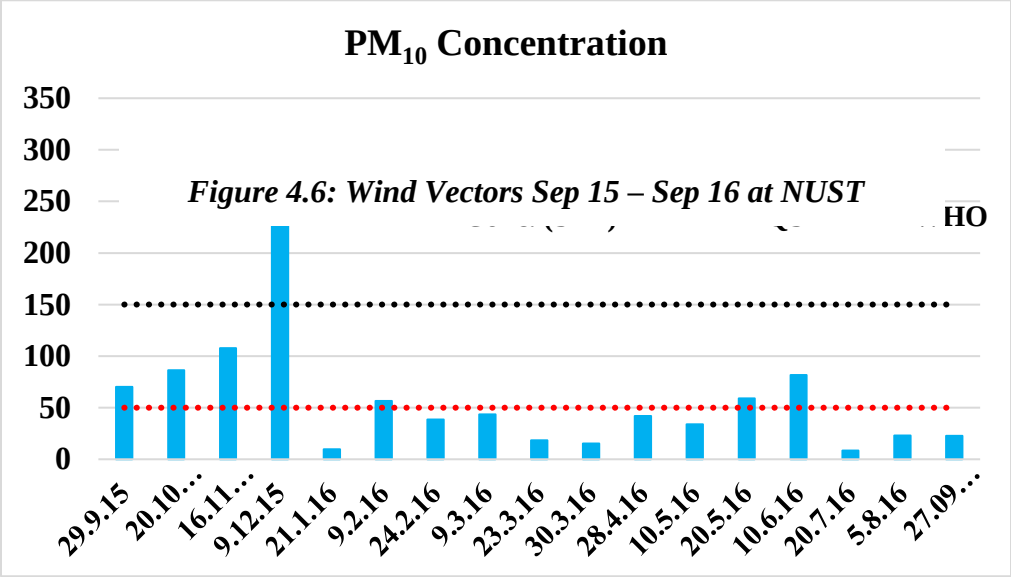

Figure 4.6: Wind Vectors Sep 15 – Sep 16 at NUST

Figure 4.7: Variation in the Concentration of PM_{10} Sep 15 – Sep 16 at NUST

show a drastic drop in January, followed by an increase in February, somewhat stabilizes through March and April, until it starts to increase in May, peaks in June, goes through yet another drastic drop in July and stabilizes through August and September. Overall the concentrations do not show a pattern. The maximum PM_{10} was observed in the months of November and December. This might be attributed to the winter season. Cold and calm weather conditions under thermal inversion during winter, result in the stagnation of local air masses. Combine this with combustion sources, like industrial activities, vehicular emissions and fuel combustion for power generation and domestic heating may result in higher fine particles in the atmosphere (Waheed et al., 2012).

The minimum concentration was observed in July and may be attributed to extensive rains before the sampling period. Precipitation tends to wash out the atmosphere, resulting in lower PM_{10} concentration.

Unit ($\mu g/m^3$)	Mean	SD	Maximum	Minimum
Overall	59.28	66.40	291.43	8.37
Summer	47.44	28.03	86.43	8.37
Winter	72.59	93.80	291.43	9.61

Table 4.2: Variation in Seasonal PM_{10} Concentration Sep 15 – Sep 16 at NUST

Table 4.2 shows the means and standard deviations as well as maximum and minimum values of PM_{10}, both overall and seasonal. Although the mean values for overall PM_{10} measurements do not differ significantly with the seasonal values. But there is a considerable difference in standard deviations, with winter showing a higher standard deviation than the summers. Both the maximum and minimum values were recorded in summer. Another study (Bulbul et al., 2018) conducted within Islamabad to ascertain PM_{10} and during winter fog found an average concentration of 177.33 $\mu g/m^3$, the overall measurements falling within the range of 123.59 $\mu g/m^3$ – 202.65 $\mu g/ m^3$.

The comparison between summer and winter concentrations of PM_{10} is depicted in Figure 4.8. The seasons have broadly been categorized as a) summer **(April – October)** and b) winter **(November – March)**. There seems to be no clear seasonal pattern. Except for a peak in December in winter, and three in summer, there is not much difference in the PM_{10} concentrations throughout the sampling period.

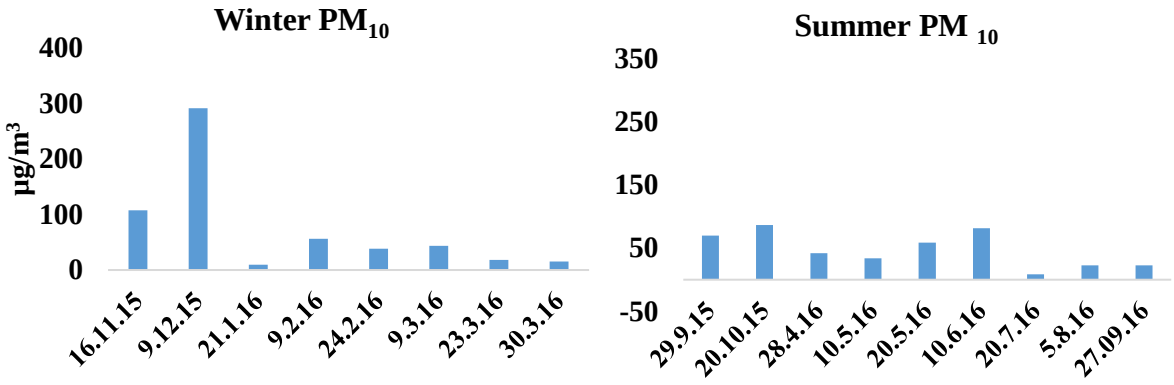

Figure 4.8: Seasonal Variation in PM_{10} Concentration

This is in line with the findings of *Waheed et al.* (2012), who studied $PM_{2.5}$ and $PM_{2.5\text{-}10}$ in the Airport Housing Society, Rawalpindi (Pakistan) and found that fine PM concentrations were comparatively higher in the winters. But no considerable seasonal variance could be observed for $PM_{2.5–10}$ and SPM at the study site. Though the difference between the averages of the current study and the Airport study (144 ± 55.4 µg/m^3) is huge, the conclusion is still relevant in this context.

4.2.1 PM_{10} and Meteorology

This section discusses the possible relationships between meteorology and PM_{10}. The graphical

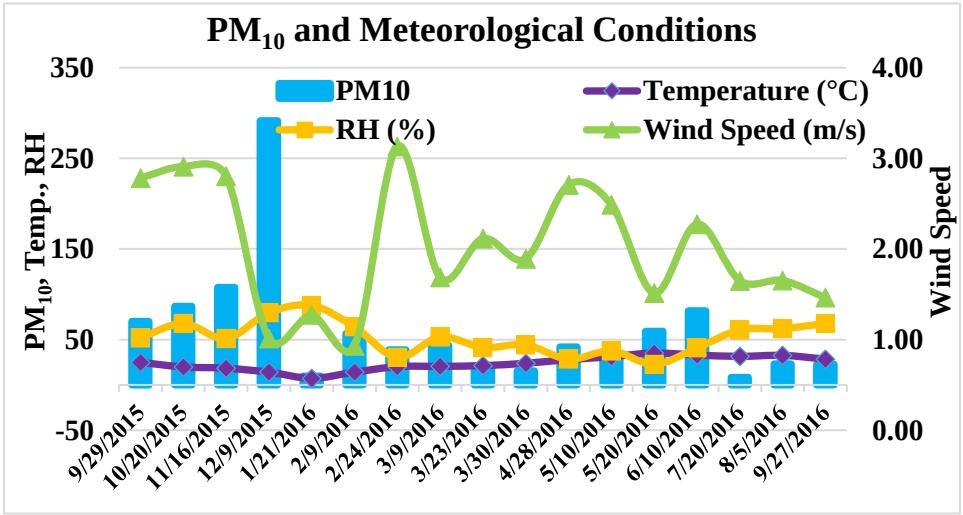

Figure 4.9: Changes in PM_{10} Concentration Compared to Meteorology

representation of the relationship between PM_{10} and meteorology, including air temperature, relative humidity and wind speed is shown in Figure 4.9.

PM_{10} increase with an increased relative humidity and shows a decline as the relative humidity drops. Few exceptions were observed, like on 21st January, 20th May and 20th July. On the **21st of January** though the relative humidity was second highest during the entire sampling period, which is 87.55 %, but the PM_{10} concentration is second lowest in this period. No clear reasons for this anomaly could be understood. **20th of May** showed a slight peak in PM_{10}, compared to concentrations during a few previous samplings. Even though the relative humidity was at its lowest at 22%, wind speed showing a dip with 1.51 m/s and might have led to the accumulation of particulate matter. **20th July** saw the lowest concentration of PM_{10} during the entire year. Being one of the three days when the PM_{10} did not show a direct relationship with relative humidity and inverse relationship with wind speed.

4.2.2 Hybrid Single Particle Integrated Trajectory (HYSPLIT)

HYSPLIT model developed by the National Oceanic and Atmospheric Administration, is used to compute the air parcel trajectories. ARL READY's online system (https://ready.arl.noaa.gov/HYSPLIT.php) allows to interactively run the model and download the results. For this study 0.5° GDAS meteorological data was selected, the receptor height was chosen to be 50 meter AGL, whereas the model was run for 48 hours prior to the sample collection. The model was run opting for different colors for each trajectory starting at a specific height. Legend at the bottom of each backair trajectory shows both the trajectories starting at varying heights and the heights they attained during their journey before they reached IESE.

The air parcels arriving on-site on the 23rd and 29th of September can be seen in the Figure 4.10. The first Backair trajectory shows that the wind came from the eastern side, originating from Rajasthan and Haryana (India), passing over the Indian Punjab, crossing Pakistani Punjab and arriving at IESE.

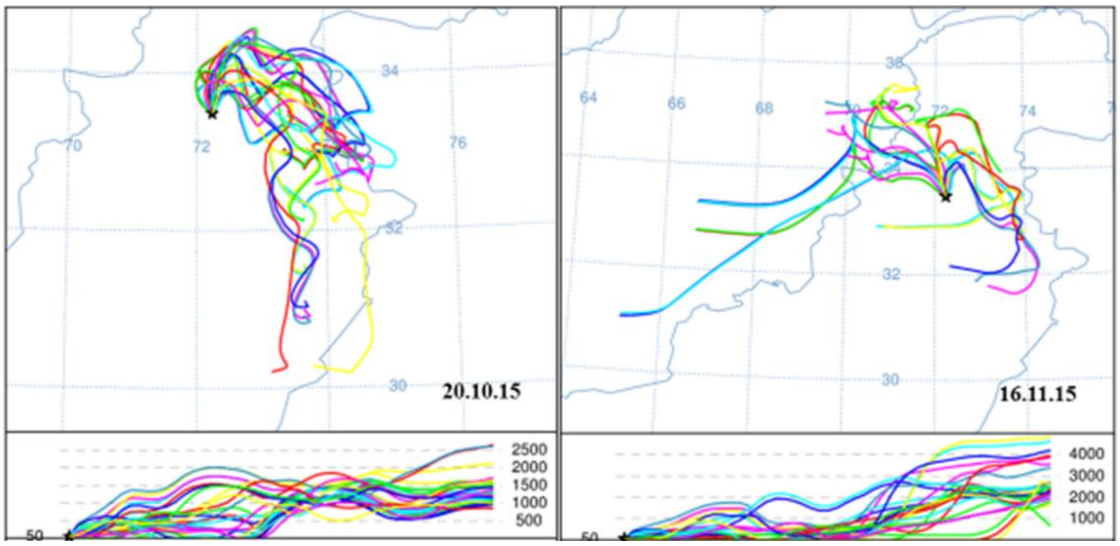

Figure 4.10: Backair Trajectories for September 2015

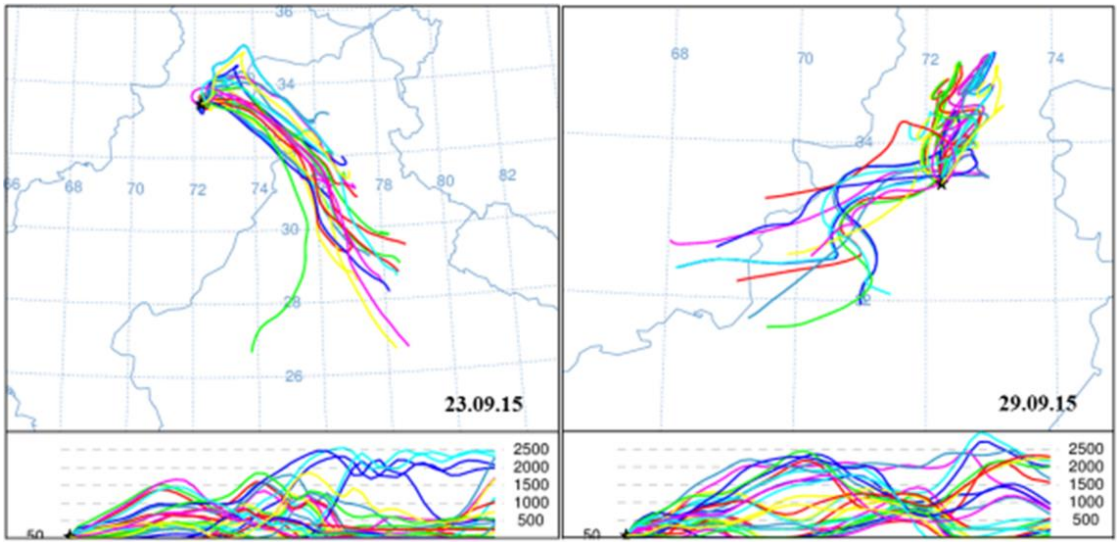

Figure 4.11: Backair Trajectories for October and November 2015

Whereas those arriving from the north-east originated in Himachal Pradesh, passed over Indian Held Kashmir, then Azad Jammu & Kashmir, (AJK) moved up north before arriving at the site. The back trajectory analysis for 29th September shows that the air parcels originated in the west (Afghanistan), south-west (Balochistan), Khyber Pakhtoonkhwa and Punjab. All passing over KPK before reaching the destination.

The first backair trajectory in Figure 4.11 shows the pathway of air parcels for 20th October. All these air masses originated within Punjab (Pakistan), some of those passing over AJK and IHK, to return and go over KPK before arriving at IESE monitoring site. On the 16th of November the winds came from multiple direcions; some of those from the eastern, western as well as north-western sides. In the East they came from Punjab (Pakistan), taking a detour over KPK before arriving in Islamabad, whereas the winds coming from west and north-west came from Afghanistan (most winds originating there).

The backair trajectories for December and January can be seen in Figure 4.12. December showed one of the highest PM_{10} concentration. A look at this map shows that the contributions were entirely regional. With air parcels coming from north-eastern side from Gilgit-Baltistan, western side(KPK) as well as Punjab. There seems to be fierce air mixing, suggesting that the wind might have re-suspended the aerosols in the air, resulting in the high concentration. On the 21st of January the wind parcels seem to be travelling over long distances. Coming from the west (Afghanistan) and north-west (Tajikistan, Kirghizstan and Kazakhstan).

Figure 4.13 shows the backair trajectories for the month of February. On the 9th of February wind came mostly from the western side, some of it originated from Afghanistan, another part from the adjoining KPK and Punjab regions and still other sections coming from the northern side (Gilgit-Baltistan).

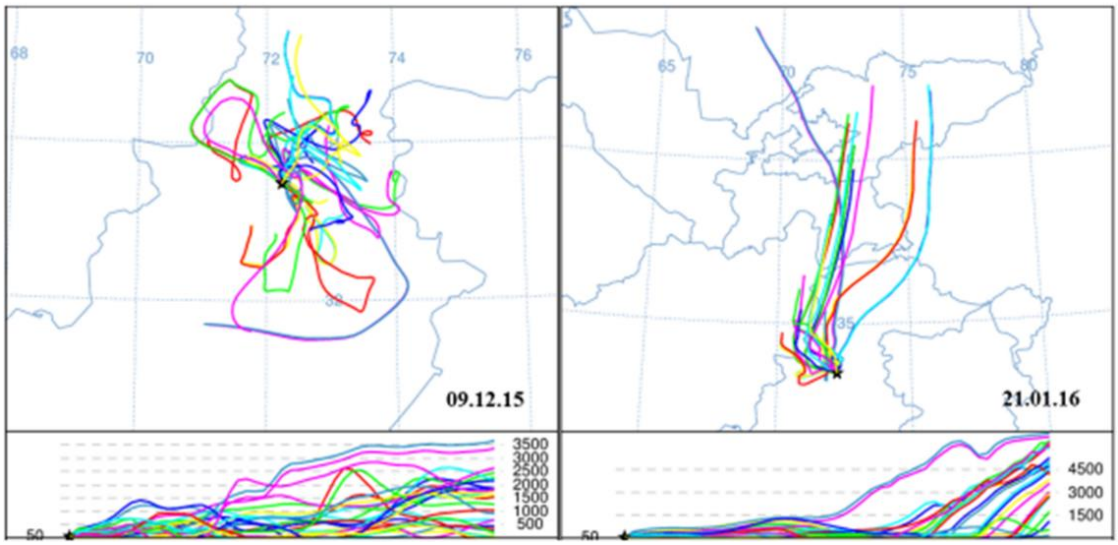

Figure 4.12: Backair Trajectories for December 2015 and January 2016

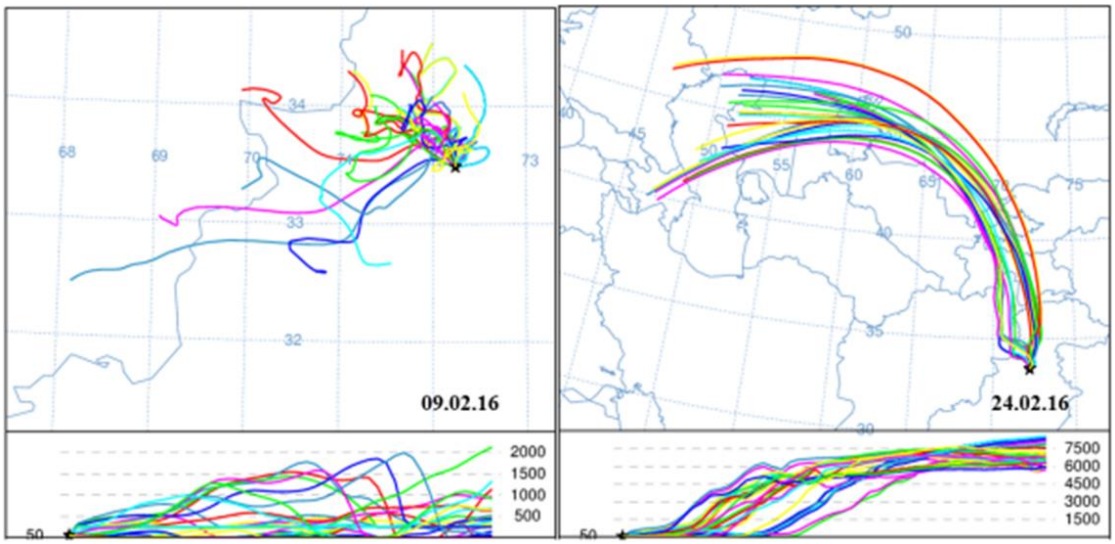

Figure 4.13: Backair Trajectories for February 2016

For the next HYSPLIT map, the air parcels appear to be emerging from the Far-East Asian States. Most of these north-western parcels originating in the Caspian Sea, as well as Azerbaijan, with exactly one trajectory originating in Russia.

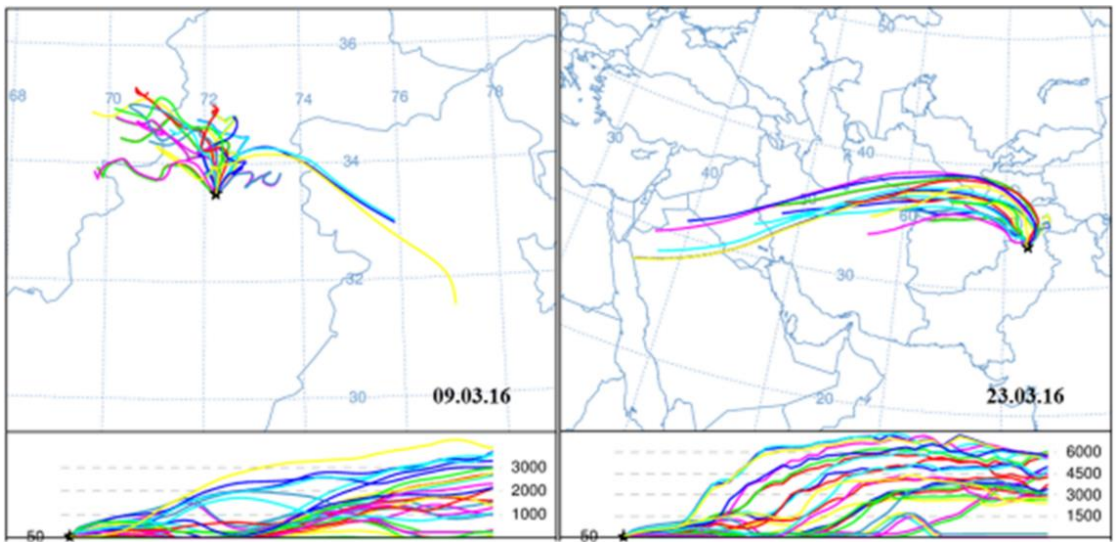

Figure 4.14: Backair Trajectories for March 2016

March continues the trend of winds dominantly coming from the western side of the site. Figure 4.14 shows the backair trajectories for the 9th and 23rd March.

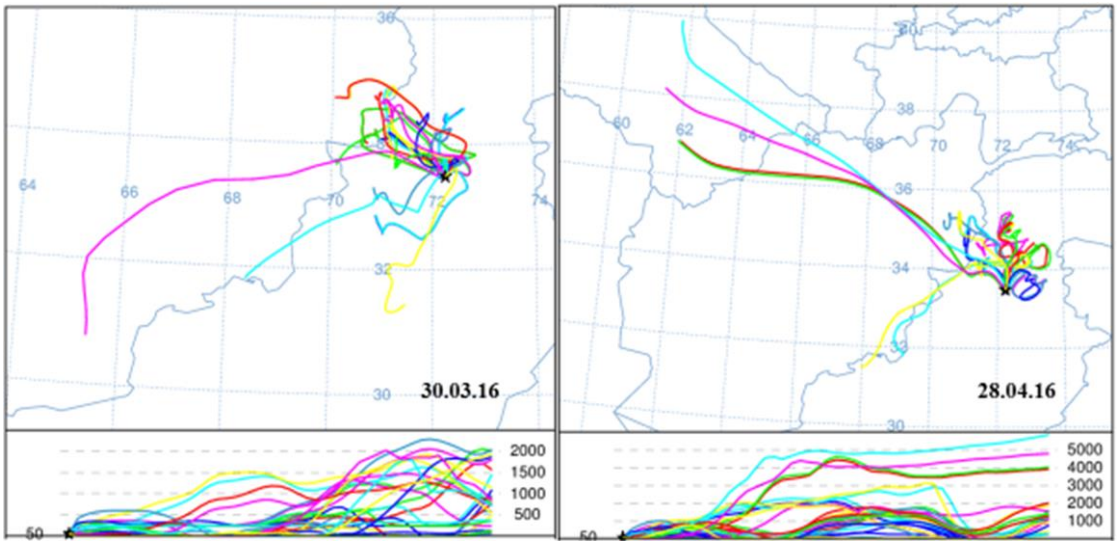

Figure 4.15: Backair Trajectories for March and April 2016

Most of these trajectories originate in the west; in Afghanistan and from the northern side in KPK, while a few arrive from the east (India) as well as from the adjoining areas. Whereas, on the 23rd the air parcels arriving at the site were long-range. The winds came from

the west; from Saudi Arabia and Iran, passing over Afghanistan, before reaching Islamabad.

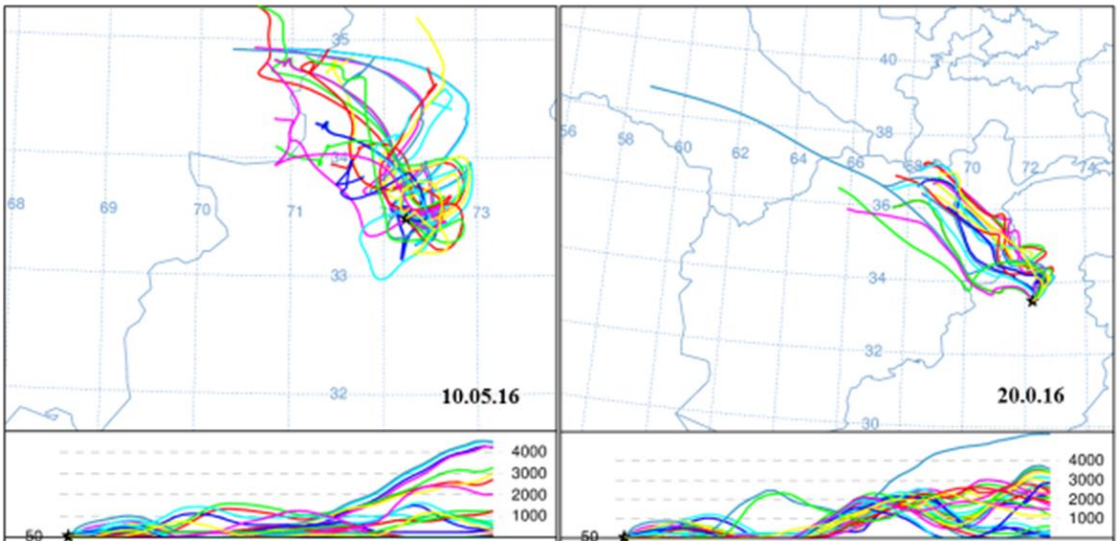

Figure 4.16: Backair Trajectories for May 2016

Figure 4.15 shows the back trajectories for 30th March and 28th April. The last of samples taken in the month of March shows air trajectories arriving from the west and south-west

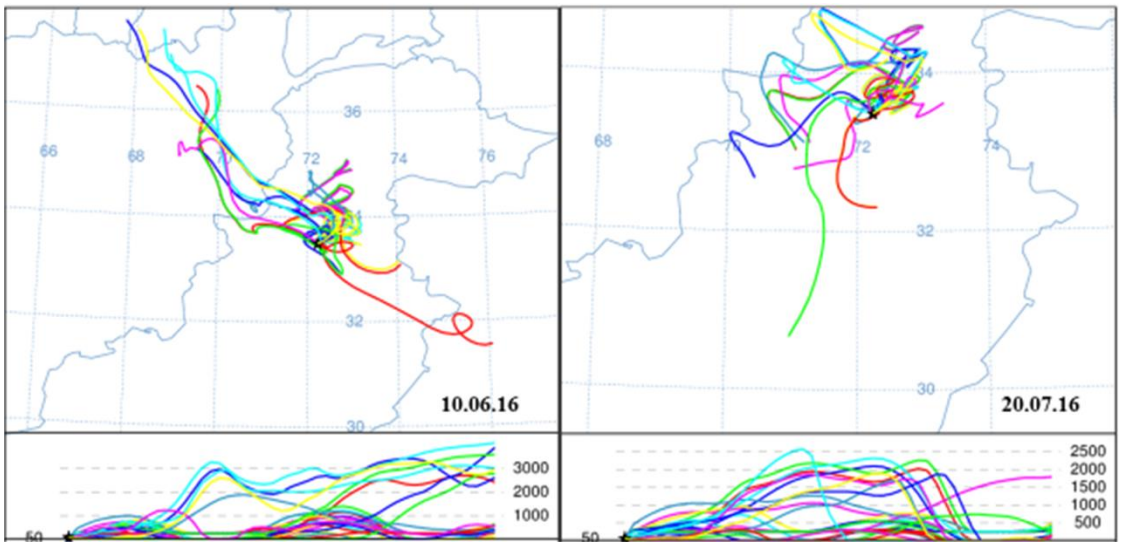

Figure 4.17: Backair Trajectories for June and July 2016

(Afghanistan), KPK and Punjab. The air parcels in April arrive from Turkemanistan and Afghanistan in the west, Balochistan in the south-west as well as the KPK and GB.

Back air trajectories for the month of May can be seen in Figure 4.16. On the 10th of May the air parcels arriving at the sampling site came from the west, from Afghanistan and the Federally Administered Tribal Areas (FATA), from the north west (KPK), as well as the adjoining areas in Punjab.

Whereas, on the 20th of May the air parcels seem to have travelled long distances before arriving at the destination. All of the air parcels coming from the west, most of these from Afghanistan. With one air trajectory travelling from Turkmenistan and Tajikistan each.

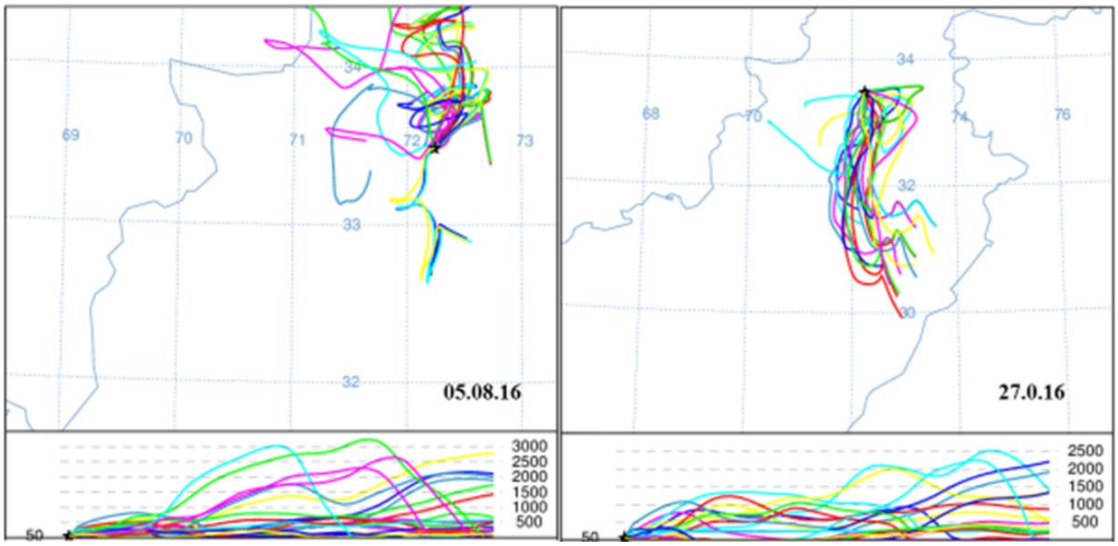

Figure 4.18: Backair Trajectories for August and September 2016

Figure 4.17 shows the pathways taken up by the air massess. In June the air trajectories came from the neighbouring Afghsnistan, Tajikkistan and Azerbaijan in the west. Locally, some of the trajectories originated in KPK. Whereas, from the eastern side, the wind came from Punjab, both the Indian as well as the Pakistani side, and AJK. For the month of July, the air trajectories originated entirely in Pakistan, mostly in the south-western (KPK) and southern (Punjab) direction. A major chunk also originated in the north (KPK) and a tiny bit in the east (Punjab).

Finally, the last pair of backair trajectories shows the air parcels arriving at the site for the months of August and September. On the 5th of August, the air trajectories show a lot of spread

in terms of direction. A lot of these originated in the western (KPK) and north western (KPK and GB) direction, while some of it came from the east and north (Punjab). On the 27th of September, almost all the trajectories originated in the north-east, in Punjab, with only a few coming from the western side, from the province of KPK and FATA.

4.2.3 Wind Rose

Wind rose is a graphical representation of the wind speed and wind direction. Differently colored spokes correspond to a specific wind speed, their length signifying the percentage of time the wind blew in a particular direction with a specific speed. Whereas, the width of these spokes refer to the wind's spread in terms of direction.

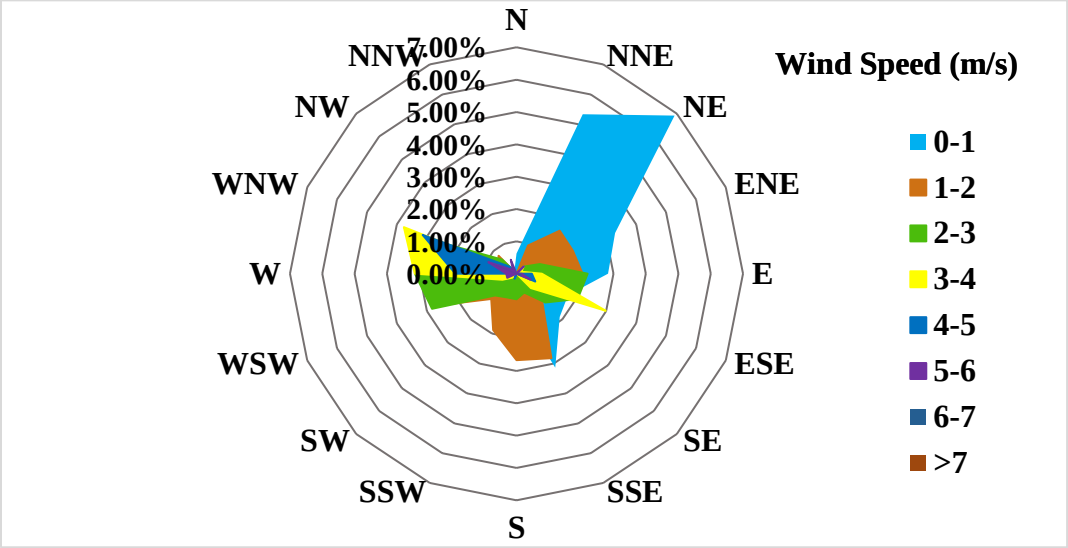

Figure 4.19: Wind Rose for the Entire Sampling Period

Figure 4.19 represents a cumulative wind rose diagram for the entire sampling period. It shows that most of the wind blew in north-eastern and north-north eastern direction, with nearly 7% and over 5% blowing below 1 m/s wind speed, roughly 2% having a speed between 1-2 m/s. Other prominent wind directions include the north-western, western and southern winds. Nearly 4% of the wind blowing in the WNW direction blew within the speed range of 3-4 m/s, roughly

3% within 4-5 m/s range and below 1% blowing with the 5-6 m/s speed bracket.

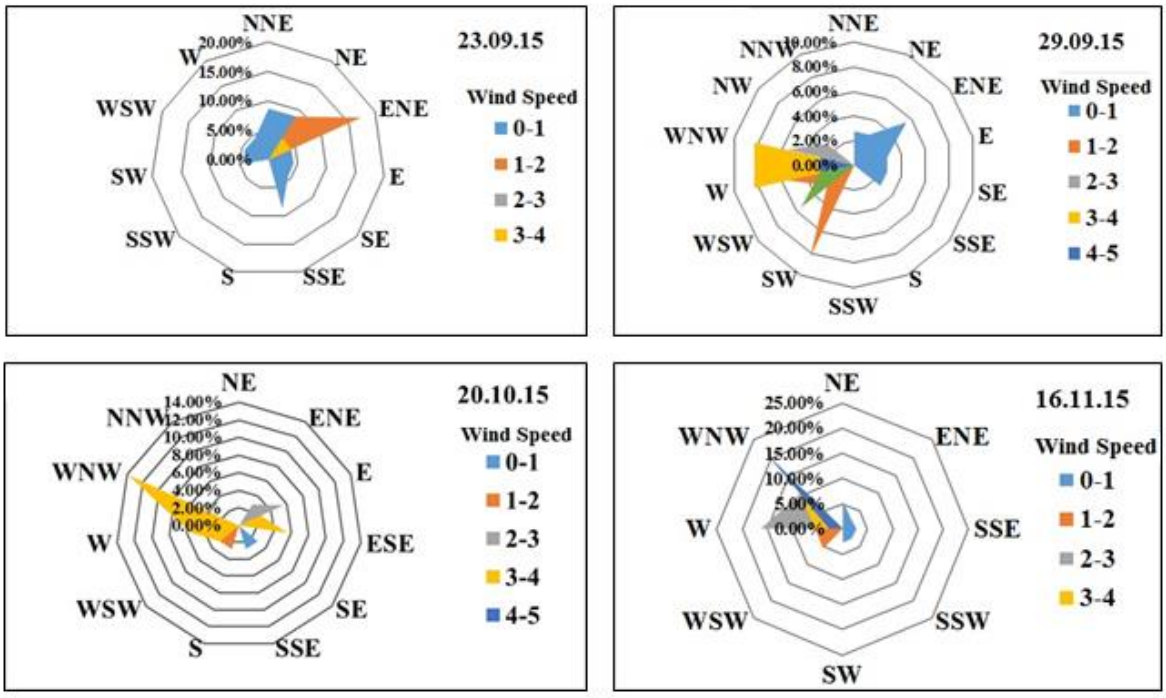

Figure 4.20: Wind Rose for September, October & November 2015

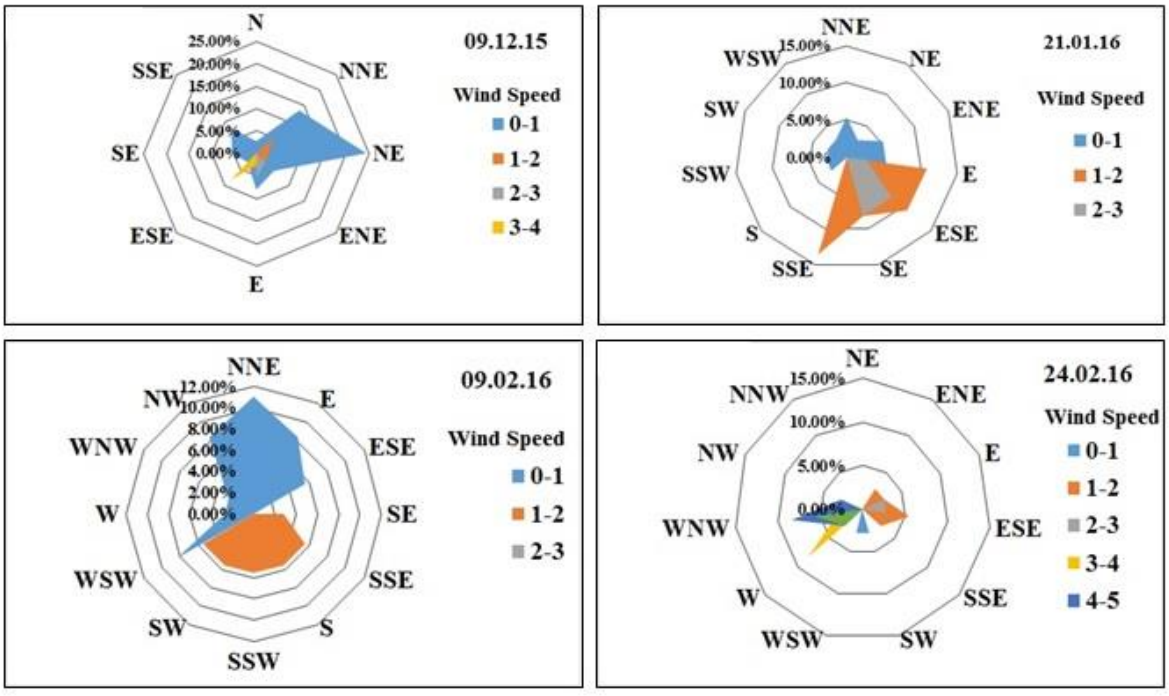

Figure 4.21: Wind Rose for December 2015, January & February2016

The third prominent wind direction is south, where nearly 3% of the time the wind blows within 1-2 m/s wind speed range.

Figure 4.20 shows the wind rose diagrams for the months September – November. This diagram shows the average wind speed and direction during the sampling period. The average wind speed had been blowing from the north-east. This happens to be the same direction where the I-9/I-10 industrial sectors are located. Also in the same direction, emerges the IJP road from the adjacent Rawalpindi city's busy Mandi Mor, connecting it to the main Kashmir Highway. Bringing poorly maintained pickups converted for passenger use and other heavy traffic into the city. Both of which could possibly have served as the sources of soot (not measured) and heavy metals (selectively measured), into the PM concentration.

On the **23rd of September**, most of the wind blew in the **east- north east** with a speed of 1-2 m/s for over 15% of the time and with 3-4 m/s for 5% of the time. On the **29th of September**, the winds were predominantly western, with each of the west-northwest and westward winds blowing with a speed of 3-4 m/s for 10%. And a southwest wind blowing with a speed of 1-2 m/s for 8 % of the time. The wind seemed to be more distributed on the **20th of October**. Nearly 14% of the time blowing in from the west-northwest direction with a wind speed of 3-4 m/s and 6% of the time from the west, falling within the same speed bin. **16th November** saw more of the west ward winds. With 20% of the winds blowing with a speed below 1 m/s from the west-northwestern direction and a little over 15% coming from the west with a speed of 2-3 m/s.

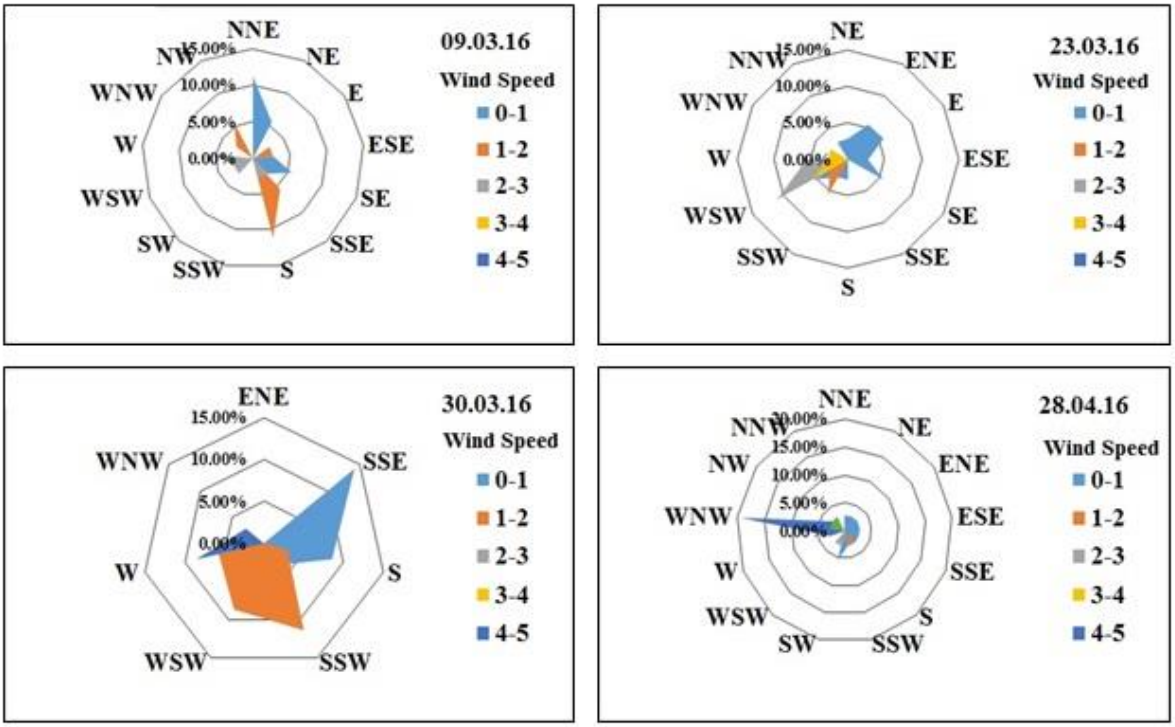

Figure 4.22: Wind Rose for March & April 2016

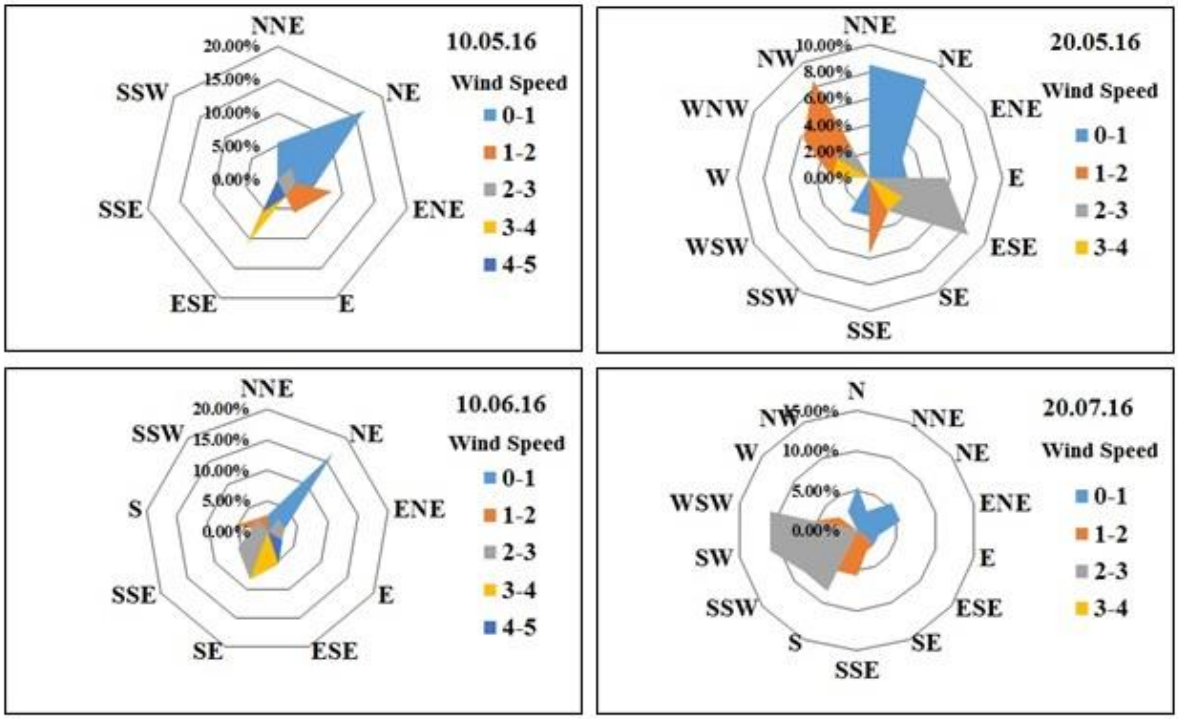

Figure 4.23: Wind Rose for May, June & July 2016

Wind rose for December, January and February can be seen in figure 4.21. On the **9th of December**, winds coming from most of the directions had mild speed, predominantly below 1 m/s. Nearly 25% of the time the winds came from northeast, whereas nearly 15% came from north-northeast. Both blew with wind speed below 1 m/s. On **21st January**, most of the winds had a speed between 1-2 m/s. For about 13% of the time the wind came from south-southeast, and 11% of the time from east and east-southeast with a wind speed between 1-2 m/s. On **9th February** the wind blew from the north-northeast direction, with speed below 1 m/s for about 11% of the time. Other winds from the eastern and northern side had a similar wind speed, whereas those coming from the southern and southwestern side had a higher wind speed (1-2 m/s). On **24th February** the wind directions ranged from the northeast to south east and west-northwest to the west. For about 7% of the time, the winds came from the west-northwest with a wind speed below 1 m/s, for nearly a similar percentage of timeme they came from west with a speed range falling between 3-4 m/s.

Figure 4.22 depicts the wind rose diagrams for the sampling site, on the days PM_{10} samples were taken, for the months of March and April. **9th March** saw winds coming in from multiple directions. For about 11% of the time the winds blew from north-northeast with a speed below 1%. On **23rd March** the winds came from east-northeast – southeast, as well as from west-southwest – south-southwest. For more than 10% of the time the winds came from west-southwest with a wind speed of 2-3 m/s. **30th March** had more of southern winds. Roughly 14% of the wind blew from south-southeast, with a speed less than 1 m/s. Whereas an 11% came from south-southwest with a slightly higher wind speed falling within 1-2 m/s bin. On **28th of April** the wind direction was more distributed and towards the higher end in terms of ed. For about 18% of the time the wind came from west-northwest, blowing with a speed within the range of 4-5 m/s.

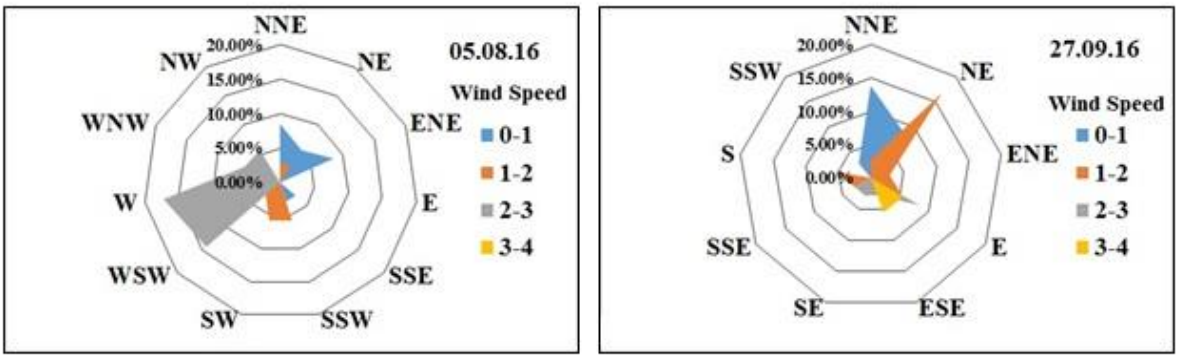

Figure 4.24: Wind Rose for August & September 2016

The wind roses for the months of May, June and July can be seen in figure 4.23. Most winds on **10th May** came from the eastern and northeastern sides. For about 17% of the time the wind blew from the northeast side with less than 1 m/s wind speed. The winds on **20th May** came from varied directions with a variety of wind speed ranges. For more than 8% of the time the wind was directed from north-northeast as well northeast with each of these blowing with a speed less than 1 m/s. For a similar amount of time the wind came from east-southeast blowing at 2-3 m/s, as well as from northwest with 1-2 m/s wind speed. The largest contribution to the winds on **20th May** came from northeast, with wind coming from that direction for over 15% of the time with a speed less than 1 m/s. Other wind directions included eastern, southeastern and southern. On **20th June** most of the wind blew with a speed of 2-3 m/s, 11% of the time from the west-southwest and southwest directions.

Figure 4.24 shows the last two wind rose diagrams which depict the directions from which the wind blew on 5th August and 27th September, with their respective speeds. On **5th August**, about 16% of the time the wind came from the western side and less than 15% of the time from west-southwest with a speed of 2-3 m/s. On the last day of sampling, more than 15% of the wind came from northeast within a speed bin of 1-2 m/s, approximately 14% of it came from north-

northeast with a speed less than 1 m/s, and roughly 3% blew in the same direction with a little higher speed of 1-2 m/s.

4.2.4 Statistical Relationships between PM_{10} and Meteorology

Atmospheric particulate matter distribution and transfer is significantly linked to meteorological parameters including temperature, precipitation, relative humidity, wind speed and wind direction. Estimating the relationship between PM and meteorological concentration could facilitate in identifying the likely sources of PM and thus help designing cost-effective

	PM_{10}	**Temp**	**Pressure**	**WS**	**WDI**	**U wind**	**V wind**	**RH**
PM_{10}	1							
Temp	-0.32	1						
Pressure	0.04	-0.85**	1					
WS	-0.27	0.22	0.10	1				
WDI	-0.40	0.01	0.21	0.54*	1			
U wind	0.20	0.13	-0.36	-0.51*	-0.94**	1		
V wind	0.39	-0.05	-0.06	-0.52*	-0.70**	0.59**	1	
RH	0.51*	-0.58**	0.26	-0.56**	-0.46*	0.34	0.35	1
*. Correlation significant at the 0.05 level (2-tailed)								
**. Correlation significant at the 0.01 level (2-tailed)								

Table 4.3: Correlation Matrix for Pearson's Correlation Between PM_{10} and Meteorology

emission control strategies (Javed et al., 2015).

Therefore, to find a statistical backing for the apparent relationships between meteorology and PM_{10}, correlation and regression analysis was performed. Results for Pearson's correlation between PM_{10}, temperature, pressure, wind speed, relative humidity, wind direction index (WDI) as well as u wind and v wind are shown in Table 4.3.

With the exception of relative humidity, PM_{10} concentration did not have a significant relationship with meteorology. Jaafar et al., 2011 found through a multiblock analysis that the PM values could best be used to predict Max and Min temperature as well as humidity. Suggesting the importance of these parameters in PM concentrations measured at a specific site, more than other parameters. Rainfall, wind speed and pressure on the other hand, were not so well predicted by the atmospheric PM datasets.

But even a correlation that is not significant suggests possibly an inverse relationship between PM_{10} and temperature, wind speed and WDI. Negative correlation with temperature could point that lower temperatures facilitate accumulation and formation of particulate matter in the atmosphere

A negative relationship with wind speed might suggest dispersion of particulate matter as the wind speed increases. Whereas, the inverse relationship with the wind direction index could mean that the dominant wind directions at the study site tend to disperse the PM, instead of resuspension or bringing the particulate. A study (Li et al., 2017) in north-east China found that the PM concentrations were negatively correlated with wind speed during all seasons when the

incidence of high speed winds was lower compared to the following year. And concluded that strong horizontal dispersion played an important role in reducing PM concentrations.

Model Summary(b)						
Model	**R**	**R^2**	**Adjusted R^2**	**Std. Error of the Estimate**		
1	.79a	0.62	0.50	60.24		
ANOVA(b)						
Model	**Sum of Squares**		**df**	**Mean Square**	**F**	**Sig.**
1	**Regression**	75921.94	4	18980.49	5.23	.01a
	Residual	47181.33	13	3629.33		
	Total	123103.3	17			
				Coefficients(a)		
	Unstandardized Coefficients			**Standardized Coefficients**		
Model		**B**	**Std. Error**	**Beta**	**t**	**Sig.**
1	**(Constant)**	13926.48	5506.45		2.53	0.025
	Temperature	-9.02	3.83	-0.81	-2.35	0.035
	Pressure	-18.632	7.64	-0.89	-2.44	0.03
	WDI	-152.882	45.37	-1.84	-3.37	0.005
	U wind	-98.776	32.01	-1.76	-3.09	0.009

Table 4.4: Regression Model Explaining the Variance in PM_{10} Concentration with Changes in Meteorology

Positive relationships with pressure, relative humidity, u wind and v wind were noted. High relative humidity (Li et al., 2017) favors the partitioning of semi-volatile species into the

aerosol. In addition, moist atmospheric conditions are normally accompanied by low boundary layer heights, enhancing PM concentrations in the near-surface layer. A positive relationship with the wind vectors; u-wind and v-wind. It must be noted that correlation by no means suggest causation, instead it shows that the concerned variables might be linked to that parameter.

A linear regression model was run to assess the potential influence of meteorological parameters over the PM_{10} concentration. All the parameters mentioned earlier were considered for the model. Then a hit and trial method was adopted to select the parameters that gave the best results. Table 4.4 shows the results for the regression analysis. It suggests that nearly 62% of the variation may be explained by the combined effect of the unit changes in temperature, pressure as well as the wind components Wind Direction Index and u wind. All these parameters have understandably a negative relationship with particulate matter. Suggesting that the PM goes down with an increase in temperature, pressure and WDI, as well as the eastern and western wind vectors (depicted by u-wind).

4.3. Heavy Metals

4.3.1 Heavy Metals Concentrations

Figure 4.25 shows the concentration of selected heavy metals in ng/m^3 found in the PM_{10} samples. Heavy metals e.g. cadmium, chromium, copper, iron, nickel, lead and zinc were analyzed for this study. Zinc was found to be the highest in concentration, followed by iron and lead. Table 4.5

shows both the mean values of the heavy metals' concentrations as well as their respective

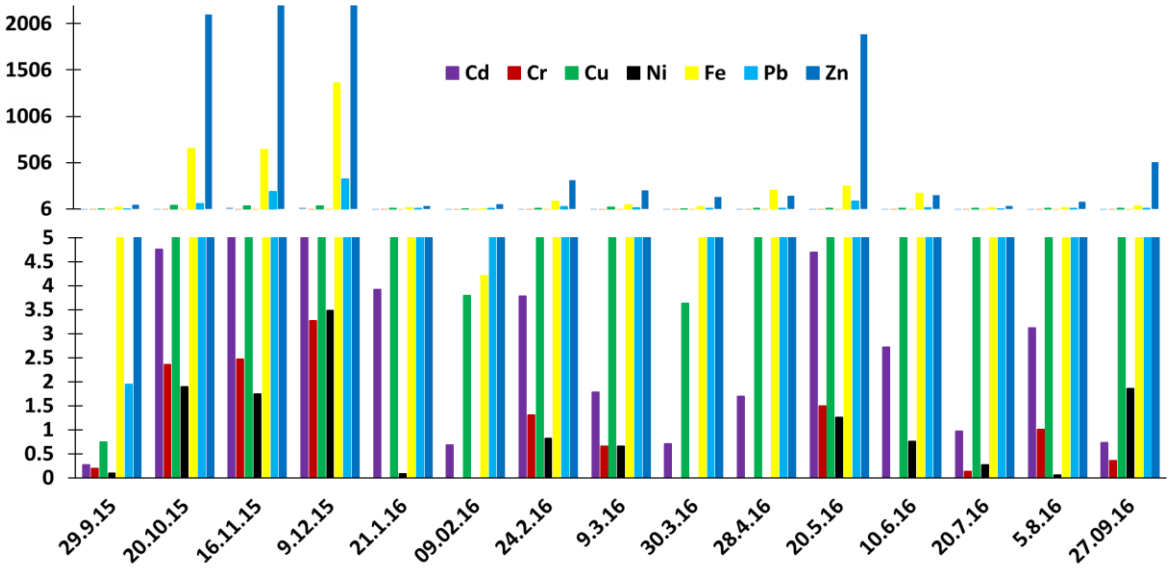

Figure 4.25: Concentrations of Selected Heavy Metals Retrieved from PM_{10} Samples

Unit (ng/m^3)	Average	SD	Max	Min
Cd	4.27	5.43	17.71	0.27
Cr	0.88	1.08	3.26	0
Cu	13.61	12.84	40.20	0.75
Fe	239.12	379.32	1367.35	4.21
Ni	0.86	1.01	3.48	0
Pb	53.03	90.79	325.63	1.95
Zn	1235.27	2199.35	6686.98	36.56

Figure 4.5: Mean, Standard Deviation and Range of Heavy Metals in PM_{10}

standard deviations. For comparison it also contains the mean and standard deviation for PM_{10}.

PM_{10} concentrations have been shown in µg/m^3, whereas the heavy metals have been shown in ng/m^3. Metals with the highest concentrations have a similarly higher degree of standard deviation, whereas those with lower concentrations like Chromium and Nickle show little standard deviation.

4.3.2 Relative Concentrations

Figure 4.26 shows the varying concentrations of **Zinc (Zn), Iron (Fe) and Lead (Pb)**, as the PM_{10} concentrations vary during each month. The heavy metals do not follow the same pattern as PM_{10}, but from January – April, the heavy metals concentrations are comparatively much lower. Also on 23rd September 2015, one of the highest PM_{10} concentrations, 295 µg/m^3, was observed. But the metals shown in this graph do not coincide in magnitude with the higher PM_{10} concentration. They show a comparatively less observation considering the difference in the PM_{10} concentrations of the two samples. But follow an upward trend onward till the drop in PM_{10} and heavy metals concentrations until January, when both the PM_{10} concentrations and heavy metals show one of the lowest concentrations. Other similar occasion occurs in July. January through June, the concentrations have stabilized except two days, on 21st January and 30th March; while a smaller peak was observed for June. The heavy metals under consideration also show a stable concentration during this period, only showing a dip in January, not following the PM_{10} drop in concentrations on the 30th of March. Overall the third low in PM_{10} concentrations and the lowest PM_{10} concentration was observed during the sampling. Besides following the patterns discussed for these metals, Zn alone shows slightly different peaks on a few occasions. Its highest concentration was observed on the 16th of November at 6687 ng/m^3, when the PM_{10}'s observed concentration is third highest at 107 µg/m^3 still considerably lower than the other two standing at 295 and 291 µg/m^3. The second peak was observed on 20th May, at 1929 ng/m^3 when the PM_{10}

concentration was 59 µg/m^3, less than the average PM_{10} concentration for the entire period. It shows another rise at the end of the sampling period with 509 ng/m^3, when the PM_{10} has stabilized at 22.8 µg/m^3.

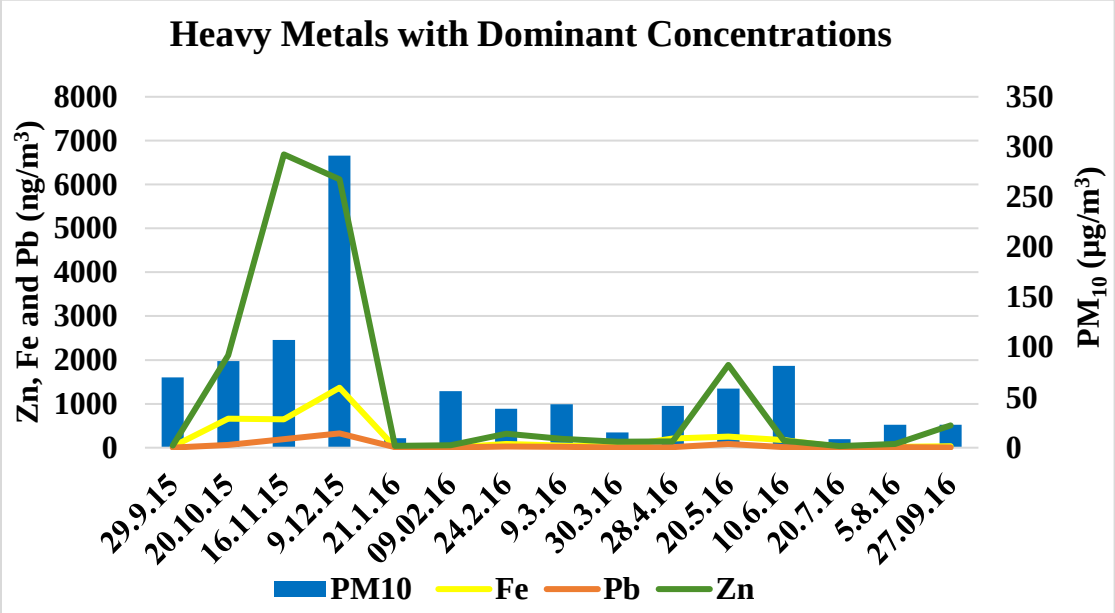

Figure 4.26: The Varying Concentrations of Fe, Pb and Zn with PM_{10} Concentration

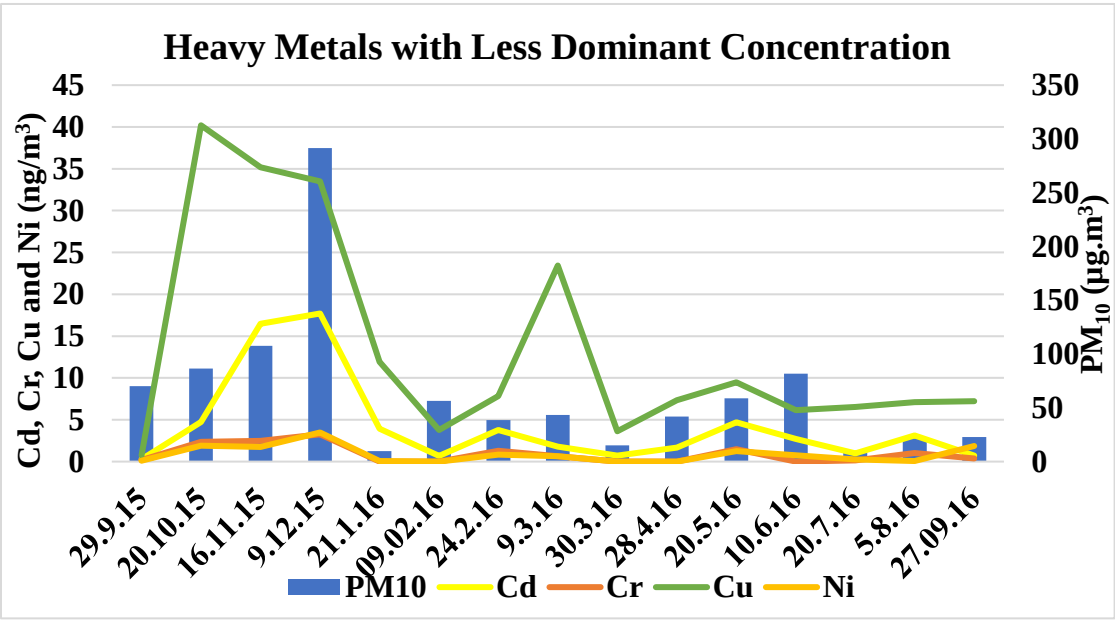

Figure 4.27: The Varying Concentrations of Cd, Cr, Cu and Ni with PM_{10} Concentration

Figure 4.27 shows the variation of heavy metals with comparatively lower concentrations as the PM_{10} concentrations vary. **Cadmium (Cd), Chromium (Cr) and Nickle (Ni)** follow almost a similar pattern. Normally their peaks coinciding with the peaks of particulate matter. Although neither show a considerable peak for 23rd September, even Cd shows much variation in its concentration. Cr and Ni have the lowest concentrations and show minimal variations. **Copper (Cu)** has the highest concentration in this group of heavy metals with comparatively lower concentrations. It shows four peaks. The first one on the 23rd of September, second peak on the 20th of October when the PM_{10} concentration measured at 86 µg/m^3, higher than the previous one but considerably lower than the two following samples. The next peak appears on the 9th of March when the PM_{10} concentration stood at 43 µg/m^3, less than the average PM_{10} concentration. The next coincides with those of Cd, Cr and Ni.

4.3.2.1 Cadmium

It has the second lowest concentration amongst all the heavy metals, the samples were analyzed for. The likely sources of cadmium at the site might include low quality coal, wood, used rubber tires as well as waste oil, used in the brick kilns. Islamabad has quite a few brick kilns in its peripheral regions. Besides, the study location lies close to Golra Mor, as well as some fringe colonies mostly consisting of tents or mud houses of the workers as well as the Afghan refugees, the semi-rural and disadvantaged population still relies on wooden resources for cooking and heating. On campus use of low grade coal for barbeque, particularly in winters (due to high demand) may also be one of the contributing factors.

4.3.2.2 Chromium

Chromium is among the lowest of concentrations of the heavy metals analyzed. It has been found to be coming from sources such as petrol and diesel combustion as well as fly ash from brick kilns. The IJP road is used to transport much of the goods coming in and out of the city. Apart from goods, it emerges from one of the busiest travelling junctions of the Rawalpindi city. With numerous buses, coaches, vans and taxis transporting people from within the city as well as from several other cities. Similarly, Kashmir Highway is a busy road. There are also vans, cars, buses and coaches which allow students, faculty and other employees to commute to and from the university. Cr can also be attributed to wood burning. Since wood is still relied upon for cooking and heating purposes among the poorer neighborhoods. The presence of Cr in the PM 10 samples may be referred to as the signature for wood smoke (Waheed et al., 2012 and Javed et al., 2015).

4.3.2.3 Copper

Copper stands fourth in terms of relative concentrations of the heavy metals and fits among the lower concertation group. The possible sources of copper might include lubricant oil, brake linings, as well as the tire wear of poorly maintained and old vehicles plying on the road (Javed et al., 2015). All of these sources besides lubricant oil are a result of wear and tear processes. Once they break free from their original sources they are released in their environment and thus are settled on road and footpaths. As more vehicles pass over those areas, or wind or any other activity might re-suspend these metals in the air. Paved road dust can thus be another possible source (Javed et al., 2015). Cu is present in brake wear dust (López et al., 2011). Using

poor quality fuels such as low quality coal, waste oil, wood, used rubber tires in the brick kilns and biomass burning releases Cu in the air (Waheed et al., 2012 and Shahid et al., 2018).

4.3.2.4 Iron

Iron has the second highest concentration amongst the analyzed metals. It is a crustal metal and (Javed et al., 2015 and Alam et al., 2014) may represent the contribution of soil as primary pollutants adding to the inventory of particulate mass. It could be in the form of wind-blown soil from the periphery loose-soil areas, separate from sources of re-suspended road dust (López et al., 2011). The suspension of soil is more likely as the city experiences frequent dry spells together with recurring dust storms (López et al., 2011 and Waheed et al., 2012). Other contributing factors include mineral dust, industrial emissions, construction activities as well as vehicular emissions (López et al., 2011 and Shahid et al., 2018).

4.3.2.5 Nickle

Nickle has the lowest concentration among the analyzed heavy metals, sharing the spot with chromium. The abrasive and wear and tear processes might yield nickel particles in the form of industrial dust (Shahid et al., 2018). It is also linked to the Ni smelters found in the peripheral regions of the study (Waheed et al., 2012). Though how much of those smelters could possibly affect the Ni concentration at the study site needs to be explored. Other possible sources might include the metallurgical industry and diesel-powered vehicles, contributing to the presence of both Zn and Ni (López et al., 2011).

4.3.2.6 Lead

Lead resides in the group of analyzed metals with relatively higher concentrations. The presence of lead may yet again be attributed to soil which serves as a reservoir for Pb. Even though the addition of lead as a knocking agent in gasoline has been banned since 2001, it is present in the soil thus becoming part of road dust and eventually of PM. (Waheed et al., 2012 and Javed at al. 2015). Vehicles emissions, tire/brake wear debris and road abrasion contaminate soil with metals especially along roads with heavy traffic loads. Where the wear products are mainly emitted to the air as coarse particles. The metals emitted through these processes include Pb and Cr. Refuse burning also releases lead in the atmosphere (Waheed et al., 2012). Since lead has been banned as a fuel additive, most of the vehicular Pb emissions are now caused mainly from wear rather than fuel combustion although fuels contain Pb at trace levels (López et al., 2011). It is also reported that refuse incineration emissions contain Pb (Waheed et al., 2012).

4.3.2.7 Zinc

Zinc has the highest concentration amongst all the analyzed metals. Its presence may be attributed to lubricant oil, brake linings, and tire wear of poorly maintained and old vehicles plying on the road (Javed et al, 2015 and Waheed et al., 2012). Other possible sources include incomplete combustion processes due to traffic and domestic burning, as well as use of low quality coal, wood, used rubber tires and waste oil as fuel in brick (Javed at al. 2015 and Shahid et al., 2018). Paved road dust may also be associated with the presence of Zn (Waheed et al., 2012). Study found (Bulbul et al., 2018) that the soil dust particle constituent of Islamabad aerosols had rich sources of zinc as well. Suggesting that a proportion might also be coming from soil and mineral sources. The presence of zinc in lubricating oils in the form of additives leads has led it to be

known as the marker for automobile tyres (Waheed et al., 2012). It is released in the atmosphere as a result of break wear, tire wear and tail pipe emission due to its presence in the motor oil (López et al., 2011). Sources for several metals overlap with the soil sources. It may be referred to frequent dry spells, dust storms and many unpaved paths that result in the suspension of dust particles in the air where they mix with other sources. (Waheed et al., 2012).

4.3.3 Correlation Between PM_{10} and Trace Metals

Table 4.6 shows the correlations coefficients for the heavy metals. Though it ranges from moderate to strong correlation, in most cases there is a strong correlation. Although correlation does not suggest causation, it does suggest a similar source. Apparently, elements that are strongly correlated indicate some common sources (Javed et al., 2015). PM has the strongest correlation with chromium, iron and nickel, suggesting these metals could be constituting a significant proportion of the total particulate matter. Iron has strong correlations with all of the metals suggesting it could have both crustal/soil dust and anthropogenic sources. Iron, lead and zinc have very strong correlation with **cadmium**. **Chromium** has the strongest correlation with copper, iron and nickel, followed by the remaining three. **Copper** is most strongly correlated with chromium and iron, followed by nickel. **Nickle** has strong relationship with chromium, followed by copper and iron. Nickel chromium and copper are marker elements of petrol and diesel combustion (Waheed et al., 2012). **Lead** is most strongly correlated to cadmium and zinc. Whereas, **zinc** is most correlated with cadmium, iron and lead.

	PM_{10}	Cd	Cr	Cu	Fe	Ni	Pb	Zn
PM_{10}	1							
Cd	.680*	1						
Cr	.775**	.804**	1					
Cu	.612*	.734**	.847**	1				
Fe	.886**	.849**	.886**	.825**	1			
Ni	.860**	.598*	.813**	.662*	.811**	1		
Pb	.798**	.955**	.846**	.712**	.928**	.719**	1	
Zn	.669*	.970**	.851**	.794**	.854**	.673*	.940**	1
*. Correlation significant at the 0.05 level (2-tailed)								
**. Correlation significant at the 0.01 level (2-tailed)								

Table 4.6: Correlation Matrix Between PM_{10} and Selected Heavy Metals

	Cd	Cr	Cu	Fe	Ni	Pb	Zn
Cd	1	0.587	0.52	0.558	0.155	.841**	.797*
Cr	0.587	1	.885**	.857**	.791*	.703*	.688*
Cu	0.52	.885**	1	.950**	.731*	0.566	0.654
Fe	0.558	.857**	.950**	1	.741*	0.652	.674*
Ni	0.155	.791*	.731*	.741*	1	0.405	0.379
Pb	.841**	.703*	0.566	0.652	0.405	1	.939**
Zn	.797*	.688*	0.654	.674*	0.379	.939**	1
****. Correlation is significant at the 0.01 level (2-tailed).**							
***. Correlation is significant at the 0.05 level (2-tailed).**							

Table 4.7: Correlation Matrix Between Heavy Metals for the Summer Samples

Table 4.7 shows the correlation matrix between the heavy metals for the PM_{10} samples collected in summer. It is interesting to note that the correlation coefficients among these metals

went down as compared to the correlation coefficients attained after an overall correlation analysis of all the values.

Not only that, most of the new values are not even significant. It might be possible that the lower correlation suggests that the metals are not as closely related in summers alone. Suggesting an effect of seasonality. Iron here shows a strong correlation with just chromium copper and nickel, previously it had strong correlation with all the metals.

Table 4.8 depicts the correlation matrix for the heavy metals for the samples collected in the winter months. Here, the correlation coefficients have improved a lot. With the lowest of values observed for the correlation between Fe and Cu at 0.78, which is still very good.

	Cd	**Cr**	**Cu**	**Fe**	**Ni**	**Pb**	**Zn**
Cd	1	.940**	.875**	.922**	.910**	.957**	.980**
Cr	.940**	1	.843*	.924**	.966**	.944**	.915**
Cu	.875**	.843*	1	.787*	.822*	.827*	.873*
Fe	.922**	.924**	.787*	1	.978**	.994**	.892**
Ni	.910**	.966**	.822*	.978**	1	.973**	.868*
Pb	.957**	.944**	.827*	.994**	.973**	1	.936**
Zn	.980**	.915**	.873*	.892**	.868*	.936**	1
****. Correlation is significant at the 0.01 level (2-tailed).**							
***. Correlation is significant at the 0.05 level (2-tailed).**							

Table 4.8: Correlation Matrix Between the Heavy Metals for the Winter Samples

All of these are significant at 0.01 level, with just the exception of a few which are significant at 0.01 level. Such a high correlation where most have correlation coefficients above 0.9 it is easy to suggest that the metals are more closely related in the samples collected in winter. And that the seasonality, which consequently is related to the meteorology might have a significant influence on the make-up of PM_{10} samples. Even though we do not observe this in terms of PM_{10} or heavy metals' concentrations.

4.3.4 Enrichment Factor

In order to better understand the origins of the metals contributing to particulate matter, a relationship between the aerosols and the soil may be established by calculating the Enrichment Factors. It suggests the anthropogenic or crustal origin of these metals, by employing the elemental concentrations measured in the particulate samples.

The EF values close to 1 suggest that the metal contribution came from a crustal source, which means an anthropogenic influence might not have been significant (Shah et al., 2012). Several studies report that EF > 10 indicates the presence of an anthropogenic source of the elements, whereas EF < 10 refers to the natural resources (Şahin et al., 2016), or low enrichment. EF between 10-100 is considered moderate, and > 100 is considered to be highly enriched.

It is calculated as a ratio between the ratios of target and reference elements within the earth crust and aerosols (Shah et al., 2012). The reference metal is usually one with an overwhelming presence in nature. Although no widely agreed upon rule exists to identify a suitable reference element, typically Fe, Al and Si are considered for this purpose. Fe has been reported to be abundant in the upper continental crust by some of the studies (Şahin et al., 2016), therefore making it a suitable reference metal. In the present study, EFs were calculated using Fe as the reference element, using the relationship;

$$EF = [X/Fe]_{PM10} / [X/Fe]_{Local\ Soil}$$

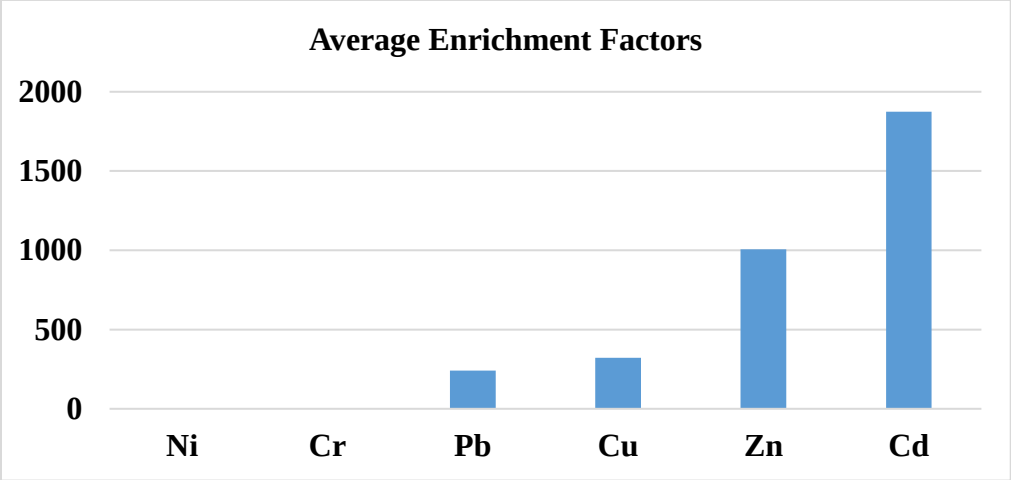

Figure 4.28: Average Enrichment Factors

Where $[X/Fe]_{PM10}$ and $[X/Fe]_{Local\ Soil}$ refers, respectively, to the ratios of mean concentration of the target element and Fe in atmospheric particulate matter and local soil (Shah et al., 2012).

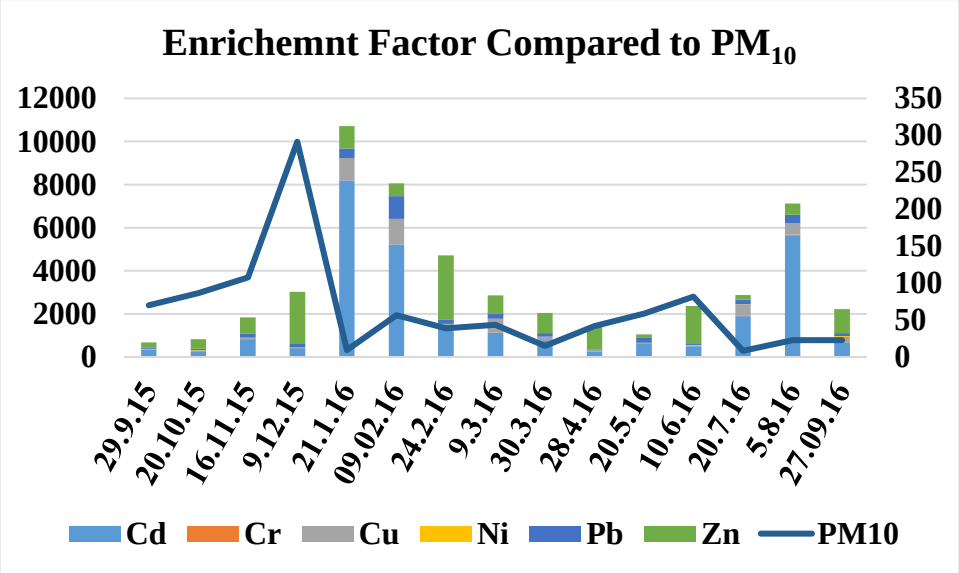

Figure 4.29: Enrichment Factors

The average enrichment factor values for the selected heavy metals can be seen in Figure 4.28. Both Ni and Cr show negligible enrichment, whereas the rest of the metals show high enrichment. Interesting to note, that lead and zinc had the highest concentrations in the aerosols, but they do not show the highest of enrichment. Even though zinc shows the second highest enrichment, it is cadmium that shows the maximum enrichment. Even though the concentration of Cd was not too high, its high enrichment suggests that though it is not very high in concentration, nonetheless it is showing high anthropogenic contributions.

Figure 4.29 shows the stacked bar graph for enrichment factors calculated for the heavy metals in the PM samples collected. The primary axis shows the enrichment factor; a unit-less parameter, whereas the secondary axis shows the PM_{10} concentration in $\mu g/m^3$. And it seems that the enrichment factor not only varied across the samples it seemingly followed a pattern of its own, not coinciding or directly conflicting with the observed peaks and troughs of the particulate matter. It actually coincides from 29th Sep – 16th Nov, but then shows lower enrichment on 9th Dec, the date with one of the highest aerosol concentration recorded. Followed by very high enrichment for Cd and Cu, though the aerosol concentration was at its lowest. On the 10th of May, once again the particulate matter was higher in concentration, but the enrichment for metals did not follow it. The last three samples show a relative contrast in the degree of enrichment and the concentrations of particulate matter.

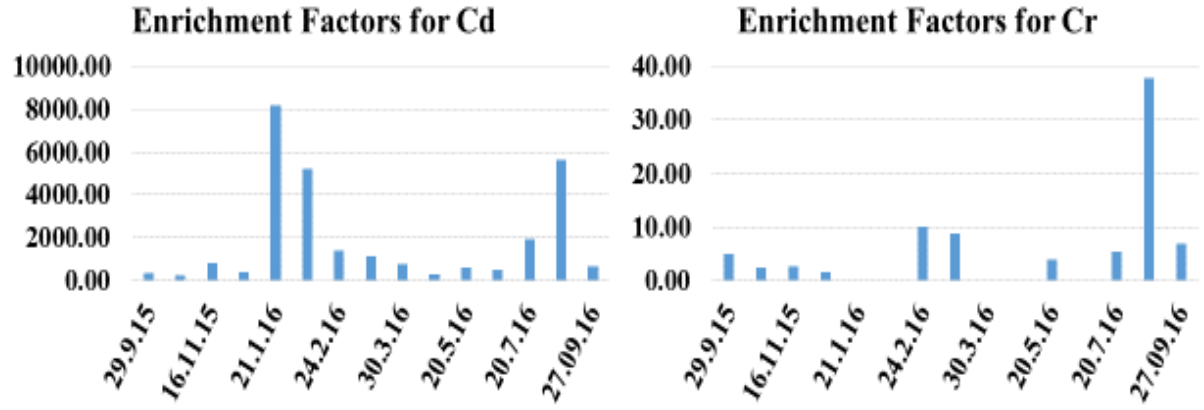

Figure 4.30: Enrichment Factors for Cadmium & Chromium Sep 15 – Sep 16 at IESE, NUST

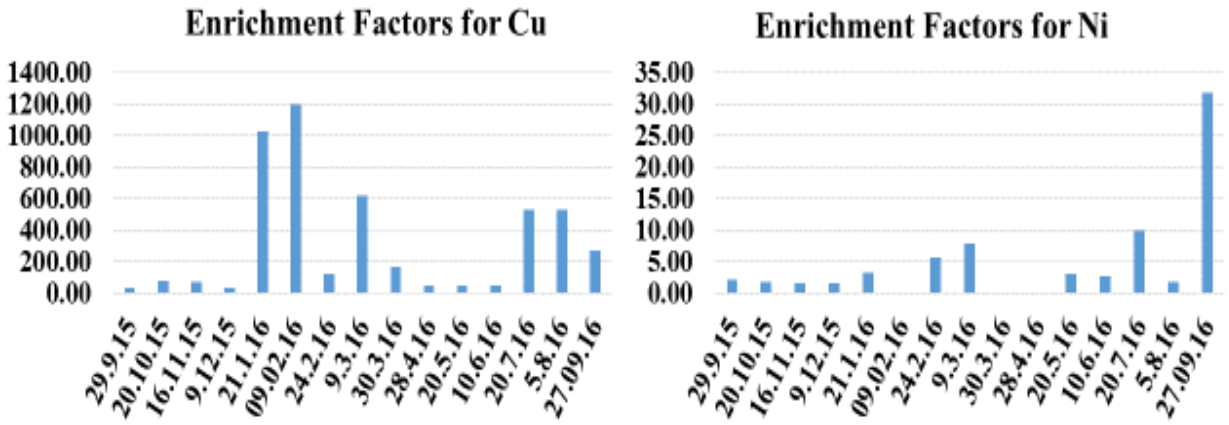

Figure 4.31: Enrichment Factors for Copper & Nickle Sep 15 – Sep 16 at IESE, NUST

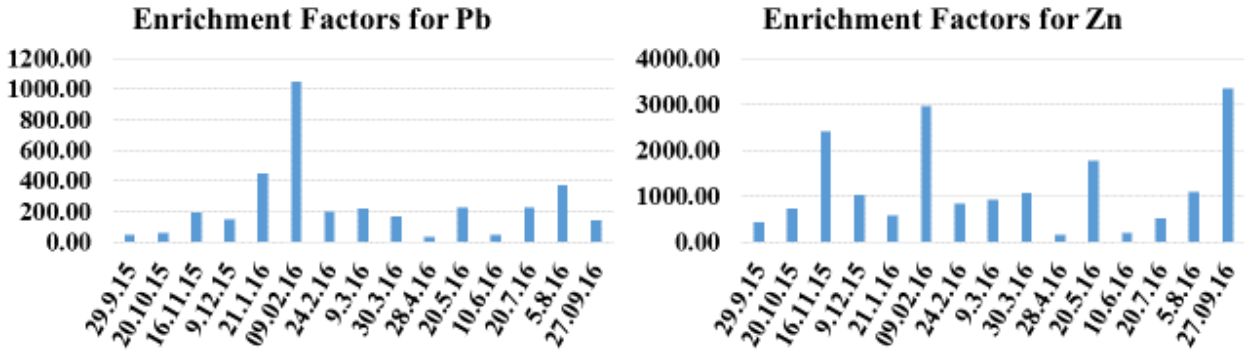

Figure 4.32: Enrichment Factors for Lead & Zinc Sep 15 – Sep 16 at IESE, NUST

Figures 4.30 – 4.32 show the EFs of the individual elements, across the sampling period. Cadmium, copper and lead show one similarity in terms of pattern, all three show peaks on 21st Jan and 9th Feb, with Zinc showing a peak only on 9th Feb. Even though the particulate concentrations were not too high. In a similar fashion, Cadmium, Chromium, Copper and Lead show peaks on 5th August. Here again the particulate concentrations had stabilized at levels less than half of the average concentration. It might be possible that a specific local activity might be contributing to these metals' enrichment higher than that found in the crustal resources.

4.4 Aerosol Optical Depth

Aerosol Optical Depth is a satellite product and is a column integrated quantity which can be used as a proxy for aerosol concentration levels (Bulbul et al., 2018). It is a unit less measure of the extinction of light as it transcends through the atmosphere. Lesser AOD values suggest a clearer atmosphere, whereas higher values suggest that the air had higher loads of aerosols, resulting in frequent absorption as well as scattering of light. Daily Level-2 AOD data was retrieved from Aqua Satellite's MODIS Collection 6 data. The DB algorithm retrieves AOD at 1 km-resolution and then aggregates them to 10 km resolution (Bulbul et al., 2018).

For the purpose of this research data was retrieved from MODIS (or Moderate Resolution Imaging Spectroradiometer), aboard the Aqua satellite. Figures 4.32 – 4.36 show the AOD maps for Islamabad Capital Territory and Rawalpindi District. The area depicted with a thicker boundary represents Islamabad, whereas the surrounding area encompasses the Rawalpindi

district. The triangular point shows IESE (NUST), the site where the ground samples were taken.

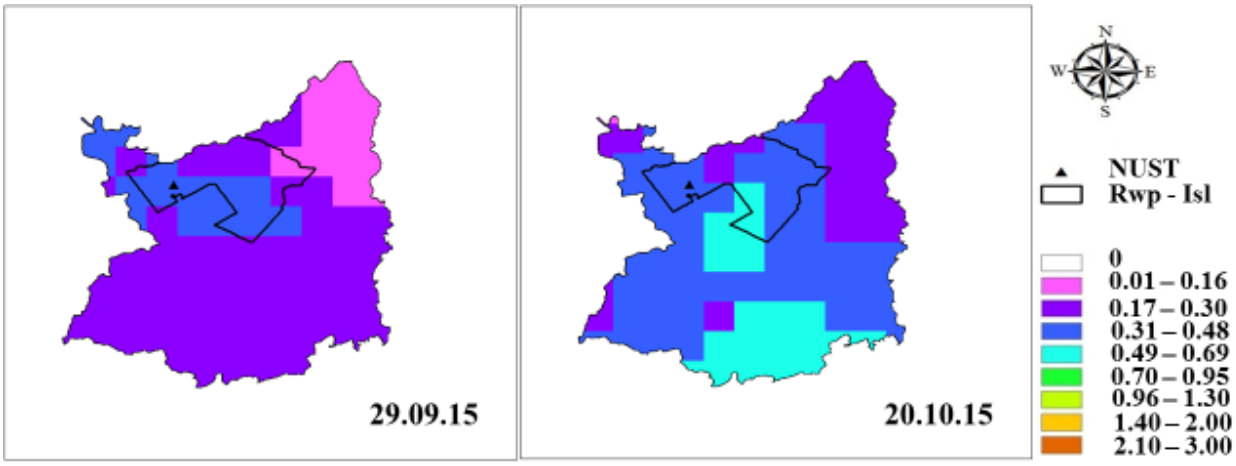

Figure 4.33: AOD Maps for September and October 2015

Figure 4.34: AOD Maps for November and December 2015

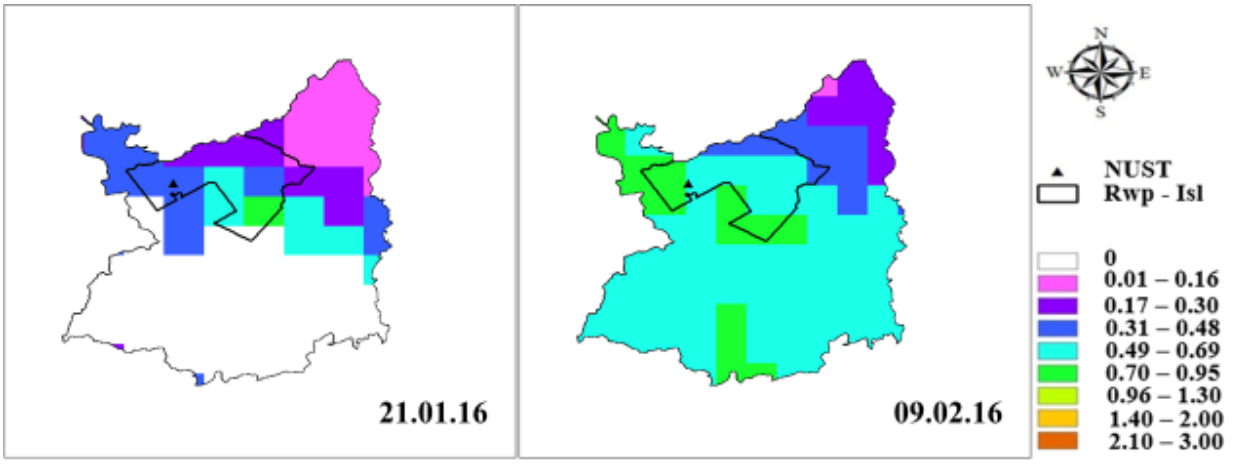

Figure 4.35: AOD Maps for January and February 2016

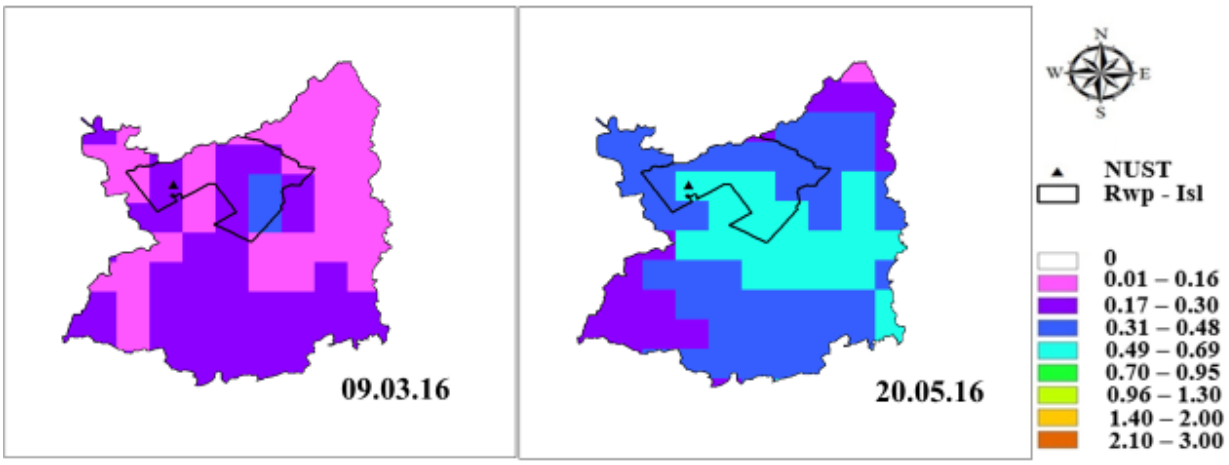

Figure 4.36: AOD Maps for March and May 2016

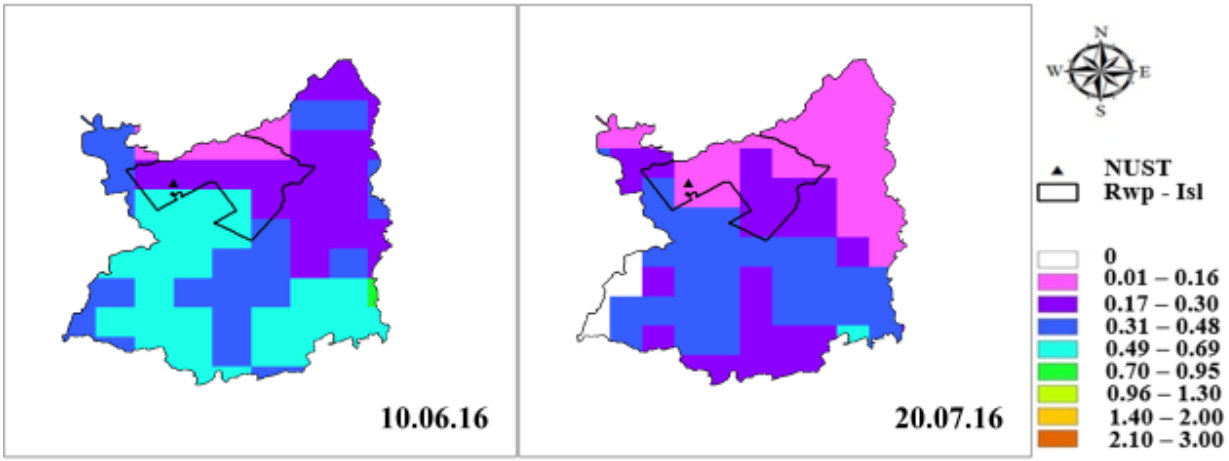

Figure 4.37: AOD Maps for June and July 2016

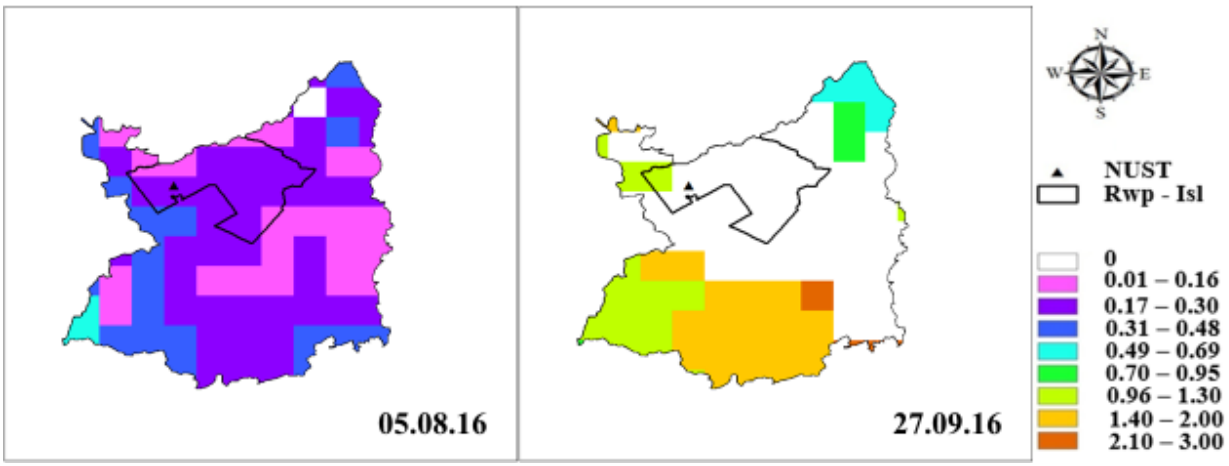

Figure 4.38: AOD Maps for August and September 2016

The raster values for this point were used to identify a correlation with the ground particulate matter. Studies have compared ground level PM concentrations to the AOD observed by MODIS on board Terra and Aqua Satellites across the globe which yield varying results with the correlation coefficients (R values) between 0.12 – 0.9 and higher for $PM_{2.5}$ and from 0.2 – 0.6 and above for PM_{10} (Zeeshan and Oanh, 2014). The **correlation coefficient** for the present study between AOD and PM was **0.49** at 0.05 significance level. It is a reasonable value according to reported literature and suggests it that the MODIS/Aqua may be used for aerosol observation in Islamabad.

Chapter 5

Conclusions and Recommendations

5.1 Conclusion

The study aimed to investigate the state of air pollution in terms of the particulate matter (PM_{10}), using both ground monitoring as well as satellite observation. For the sake of ground monitoring, PM_{10} samples were collected on IESE rooftop. Due to resource limitation, the number samples taken to study the air quality was very limited. MODIS data from Aqua satellite was used to generate the aerosol optical depth (AOD) maps. Correlation was calculated among the two data sets to assess the suitability of the satellite data for PM monitoring. To further understand the effect of pollutants on the formation of particulate matter, the collected PM samples were analyzed for heavy metals like, copper, cadmium, chromium, nickel, lead and zinc. To identify the anthropogenic or natural sources of the PM, enrichment factor (EF) was calculated. Meteorology has a profound effect on the formation, dispersion and distribution of particulate matter. Therefore, the relationship between PM, the heavy metals and meteorology was identified and tested statistically.

1. The PM_{10} concentration exceeds the national environmental quality standards (NEQS) at only one occasion (120μm^3 daily) in September and December 2015, whereas 41% of the PM_{10} concentrations exceeded WHO guidelines surpasses the World Health Organization (WHO) standards for ambient air at eight instances. The overwhelming majority of these incidents occurred during the winter season. Besides these incidents of higher PM_{10} (WHO standards), there is no evidence of effect of seasonality on PM_{10} concentration.
2. HYSPLIT model helps identify the air masses reaching at the study site, which could suggest the influence of long range air masses over PM concentration. There has been no apparent

relationship between the origin of air masses and the PM concentration. The air masses were coming from local, regional and international locations.

3. Wind rose were created to visually locate the dominant wind speed and wind direction during the sampling period. Most of the winds were coming from the north and northeastern directions, and the dominant wind speed fell within the 0-1 m/s speed bin. The other lesser prominent wind direction was the western direction. Since the industrial sectors, as well as the IJP road bringing heavy traffic, including the damaged and poorly maintained vehicles into the city, lie in the northeast of the study site. It might be implied that they had role to play in the observed PM concentrations as well as its constituents.
4. PM_{10} is found to have the strongest correlation with Cu, Fe and Ni. And a negative correlation with temperature, WDI and wind speed. This indicates that both wind speed and wind direction disperse the PM_{10}, whereas temperature might relate both in terms of air stagnation or the relationship with certain industries such as brick kilns which might be operating in winter.
5. Among the analyzed heavy metals, Zn has the highest concentration, whereas both Ni and Cr lie at the bottom. NEQS for Pb in ambient air stands at 1.5µg/m^3, none of the observations was found to be going beyond this limit. Heavy metals in the coarse PM_{10} are considered to be the results of crustal/soil or marine sources as well as the product of mechanical or abrasive processes. Either releasing the metals as vapors, later condensing into bigger particles or as minor particles as a result of wear and tear.
6. The highest concentration for metals was found to be for **Zn**, and its likely sources include poor quality coal, or used rubber tyres and waste oil used as fuel, lubricant oils for vehicles. It is also a marker metal for tyre wear. The possible contributing sources to **Fe** might include

the crust or mineral sources, construction as well as tyre wear, or mechanical dispersion from vehicles. **Pb** was previously used as an anti-knocking agent in fuel. Though banned, it might still be present in the soil, as a remnant and become part of road dust. **Cr** could be contributed by petrol and diesel combustion, as well as domestic wood burning and fly ash from the brick kilns. **Cd** likely sources include low quality fuels such as low-grade coal, as well as refuse burning in the brick kilns. **Ni** could likely be contributed by the Ni smelters or as Ni dust as a result of industrial processes. Cu is used in several electronic gadgets and vehicles and may be released by mechanical abrasion and tyre wear besides Ni. Further; Cd, Cr and Cu are also linked to biomass and refuse fuel burning.

7. Fe is highly correlated with all the metals. Cd is highly correlated with Fe, Pb and Zn. Cr with Cu, Fe and Ni. Pb with Zn. Such relationships suggest a common source of origin. In an attempt to identify the possibility of seasonality among the metals, they were correlated with each other for winter and summer seasons. The correlation was much stronger in winter, whereas in summer not only was it relatively weak, it was not even significant in some cases. Therefore, the season might have played a role, which needs to be explore in more detail.
8. Cd showed the highest enrichment factor (EF), followed by Zn, Cu and Pb. There was little to no enrichment for Cr and Ni. The enrichment also varied along the sampling period. The highest enrichment was observed during January and February, to a lesser degree in the August as well. So, the anthropogenic element does not seem to follow the same pattern as the PM or metals' concentration.
9. MODIS Aqua was found to be a good resource to prepare Aerosol Optical Depth (AOD) maps, as surrogates for PM. The correlation coefficient was close to 0.5 and significant.

5.2 Recommendations

1. The study could be used as foundation for future research, to better understand PM_{10} and the role they play in our environment. Better results could be achieved by increasing the frequency of sampling, increasing the sampling site could also be very helpful, though limited by budget constraints.
2. Non-destructive means such as INAA and PIXE could be used to get much more data without losing the original sample. The remainder could be used to identify the water-soluble ions to identify what were the dominant PM_{10} constituents in Islamabad.
3. Strategic planning about future sampling, including more size fractions could help identify problems, such as smog and haze early on. Studies may also be designed to study the role of PM_{10} in likely changes in cloud formation and its dynamics and its effects on precipitation.
4. Volatile component of the PM_{10}, should be studied to understand the dynamics in a rapidly developing urban environment, as more skyscrapers, shopping malls and road networks pop up across the city.

References:

Air Resources Laboratory. https://www.arl.noaa.gov/hysplit/hysplit/. 2017.

Alam, K., Mukhtar, A., Shahid, I., Blaschke, T., Majid, H., Rahman, S., Khan, R. and Rahman, N., 2014, 'Source Apportionment and Characterization of Aeorols in Lahore', Aerosol and Air Quality Research, 14: 1851-1861. doi: 10.4209/aaqr. 2014.01.0005

Alam, K., Shaheen, K., Blaschke, T., Chishtie, F., Khan, H. U. and Haq, B. S., 2016, 'Classification of Aerosols in an Urban Environment on the Basis of Optical Measurements', Aerosol and Air Quality Research. 16: 2535–2549, 2016. doi: 10.4209/aaqr.2016.06.0219

Almeida, S. M., Ramos C. A. and Almeida-Silva, M., 2015, 'Exposure and inhaled dose of susceptible population to chemical elements in atmospheric particles', J Radioanal Nucl Chem, DOI 10.1007/s10967-015-4673-5

AQUA, https://aqua.nasa.gov/. Last updated: May 04, 2018. NASA Official: Claire Parkinson

Bansah, K. J., Dumakor-Dupey, N. K. and Assan, E., 2016, 'Ambient Particulate Matter – A Review', 4th UMaT Biennial International Mining and Mineral Conference, pp. ES 44-54.

Bari M. A. and Kindzierski, W. B., 2016, 'Eight-year (2007–2014) Trends in Ambient Fine Particulate Matter ($PM_{2.5}$) and its Chemical Components in the Capital Region of Alberta, Canada', Environment International. 91 122–132.

Boss, C. B. and Fredeen, K. J., 1997, 'Concepts, Instrumentation and Techniques in Inductively Coupled Plasma Optical Emission Spectrometry' The Perkin-Elmer Corporation.

Bulbul, G., Shahid, I., Chishtie, F., Shahid, M. Z., Hundal, R. A., Zahra, F., Shahzad, M. I., 2018, 'PM_{10} Sampling and AOD Trends during 2016 Winter Fog Season in the Islamabad Region, Aerosol and Air Quality Research, 18: 188–199. doi: 10.4209/aaqr.2017.01.0014.

Compendium Method IO-2.1, 1999, 'Sampling of Ambient Air for Total Suspended Particulate Matter (SPM) and PM_{10} Using High Volume (HV) Sampler', Center for Environmental

Research Information of Research and Development. U.S. Environmental Protection Agency. Cincinnati, OH.

Compendium Method IO-2.1., 1999, 'Sampling of Ambient Air for Total Suspended Particulate Matter (SPM) and PM_{10} Using High Volume (HV) Sampler', Center for Environmental Research Information Office of Research and Development U.S. Environmental Protection Agency Cincinnati, OH.

Compendium Method IO-2.4, 1999, 'Calculations for Standard Volume', Center for Environmental Research Information, Office of Research and Development U.S. Environmental Protection Agency, Cincinnati, OH.

Compendium Method IO-3.1, 'Selection, Preparation and Extraction of Filter Material. Center for Environmental Research Information', 1999, Office of Research and Development U.S. Environmental Protection Agency Cincinnati, OH.

Criteria Pollutants, Idaho Department of Environmental Quality, http://www.deq.idaho.gov/air-quality/air-pollutants/criteria-pollutants/. Last Updated: March 8, 2018.

Czarnecka, M., Kalbarczyk, R. and Kalbarczyk, E., 2007, 'Variability in Particulate Matter Concentrations Versus Precipitation in Pomerania Region', Polish Journal of Natural Sciences, 22(4): 645-659. DOI 10.2478/v10020-007-0055-y.

Data Support Company, https://www.dscbalances.com/whatman-filter-sheets-8-x-10-prenumbered-air-sampling-quartz-qm-a-100-pk-pn-1851-8866.html. Date Accessed: 09.05.18.

Environmental Law in Pakistan: A Short Client Guide, 2016, https://joshandmakinternational.com/environmental-law-in-pakistan/. Last Updated: 02.05.16.

Falcon-Rodriguez, C., Vargas, A. R. O., Sada-OvalleIsabel, I. and Segura-Medina, P., 2016, 'Aeroparticles, Composition, and Lung Diseases', Frontiers in Immunology 7(1). DOI: 10.3389/fimmu.2016.00003.

Frazier, S., https://modis.gsfc.nasa.gov/about/. Date Accessed: 09.05.18.

Hameed, H., 2007, ‘Severe storms on dated 23rd July 2001 Islamabad, Pakistan’, 4th European Conference on Severe Storms, Trieste, Italy, 10–14 Sept.

https://www.arl.noaa.gov/hysplit/hysplit/

Jaafar, M. Z., Khan, A. H., Adnan, S., Markwitz, A., Siddique, N, Waheed, S. and Brereton, R. G., 2011, ‘Multiblock Analysis of Environmental Measurements: A Case Study of Using Proton Induced X-ray Emission and Meteorology Dataset Obtained from Islamabad Pakistan’, Chemometrics and Intelligent Laboratory Systems 107: 31–43.

Javed, W., Wexler, A. S., Murtaza, G, Ahmad, H. R. and Basra, S. M. A, ‘Spatial, temporal and size distribution of particulate matter and its chemical constituents in Faisalabad, Pakistan. Atmósfera 28(2), 99-116.

Karagulian, F., Belis, C. A., Dora, C. F. C., Prüss-Ustün, A. M., Bonjour, S., Adair-Rohani, H. and Amann, M., 2015, ‘Contributions to cities' ambient particulate matter (PM): A systematic review of local source contributions at global level’, Atmospheric Environment. 120: 475-483.

Khokhar, M. F., Yasmin, N., Chishtie, F., and Shahid, I., 2016, ‘Temporal Variability and Characterization of Aerosols across the Pakistan Region during the Winter Fog Periods’, Atmosphere, (7) 67

Khwaja, H. A., Parekh, P. P., Khan, A. R., Hershey, D. L., Naqvi, R. R., Malik, A. and Khan, K., 2009, ‘An In-Depth Characterization of Urban Aerosols Using Electron Microscopy and Energy Dispersive X-Ray Analysis’, Clean, 37 (7), 544 – 554. DOI: 10.1002/clen.200900012.

Kim, H.J., Choi, M.G., Park, M.K., Seo, Y.R., 2017, ‘Predictive and prognostic biomarkers of respiratory diseases due to particulate matter exposure’, J. Cancer Prev. 22, 6–15.

Kim., B., Bae, C., Kim, H. C., Kim, E., Kim, S., 2017, ‘Spatially and chemically resolved source apportionment analysis: Case study of high particulate matter event’, Atmospheric Environment. 162: 55-70.

Li, X., Ma, Y., Wang, Y., Liu, N. and Hong, Y., 2017, ‘Temporal and spatial analyses of particulate matter (PM10 and PM2.5) and its relationship with meteorological parameters over an urban city in northeast China’, Atmospheric Research ,198: 185–193.

López, M. L., Ceppi, S., Palancar, G. G., Olcese, L. E., Tirao, G. and Toselli, B. M., 2011, 'Elemental Concentration and Source Identification of PM_{10} and $PM_{2.5}$ by SR-XRF in Córdoba City, Argentina', Atmospheric Environment, 45: 5450-5457. doi: 10.1016/j.atmosenv.2011.07.003

MODIS, https://modis.gsfc.nasa.gov/about/.

NAAQS Table, USEPA, https://www.epa.gov/criteria-air-pollutants/naaqs-table, Last Updated: December 20, 2016.

Naimabadi, A., Ghadiri, A., Idani, E., Babaei, A. A., Alavi, N., Shirmardi, M., Khodadadi, A., Marzouni, M. B., Ankali, K. A., Rouhizadeh, A. and Goudarzi, G., 2016, 'Chemical composition of PM10 and its in vitro toxicological impacts on lung cells during the Middle Eastern Dust (MED) storms in Ahvaz, Iran', Environmental Pollution. 211: 316-324.

National Environmental Quality Standards for Ambient Air, 2010, http://environment.gov.pk/images/rules/SRO2010NEQSAirWaterNoise.pdf.

Oxford Dictionaries. (2018). https://en.oxforddictionaries.com/definition/ischaemia.

Şahin Ü. A., Polat, G. and Onat, B., 2016, 'Mass size distribution and source identification of particulate matter metal components at four urban sites and a background site of Istanbul', Environmental Science and Pollution Research.

Salam, A., Heidi, B., Kassin, K, Ullah S. M. and Puxbaum, H., 2003, 'Aerosol chemical characteristics of a mega-city in Southeast Asia (Dhaka–Bangladesh)', Atmospheric Environment, 37: 25 17–2528.

Shah, M. H., Shaheen, N., Nazir, R, 2012, 'Assessment of The Trace Elements Level in Urban Atmospheric Particulate Matter and Source Apportionment in Islamabad, Pakistan', Atmospheric Pollution Research, 3: 39-45.

Shahid, I., Alvi, M. U, Shahid, M. Z., Alam, K. and Chishtie, F., 2018, 'Source Apportionment of PM_{10} at an Urban Site of a South Asian Mega City', Aerosol and Air Quality Research, Accepted in Press. doi: 10.4209/aaqr.2017.07.0237.

Siddique, N., Markwitz, A and Brereton, R. G., 2012, 'PIXE Analysis of $PM_{2.5}$ and $PM_{2.5–10}$ for Air Quality Assessment of Islamabad, Pakistan: Application of Chemometrics for Source Identification. Journal of Environmental Science and Health, Part A, **47**: 2016–2027. DOI: 10.1080/10934529.2012.695559

Siddique, N., Waheed, S., Daud, M., Markwitz, A. and Hopke, P. K., 2012, 'Air quality study of Islamabad: preliminary results', J Radioanal Nucl Chem. 293:351–358. DOI 10.1007/s10967-012-1674-5

Simonetti, G., Conte, E., Perrino, C. and Canepari, S., 2018, 'Oxidative potential of size-segregated PM in an urban and an industrial area of Italy', Atmospheric Environment, doi: 10.1016/j.atmosenv.2018.05.051.

Taiwo, A. M., Beddows, D. C. S., Shi, Z. and Harrison, R. M., 2014, 'Mass and number size distributions of particulate matter components: Comparison of an Industrial Site and an Urban Background Site', Science of the Total Environment, 475: 29–38.

Waheed, S., Jaafar, M. Z., Siddique, N., Markwitz, A. and Brereton, R. G., 2012, 'PIXE analysis of $PM_{2.5}$ and $PM_{2.5–10}$ for air quality assessment of Islamabad, Pakistan: Application of chemometrics for source identification, Journal of Environmental Science and Health, Part A: Toxic/Hazardous Substances and Environmental Engineering, 47:13, 2016-2027.

Waheed, S., Siddique, N., Arif, M., Daud, M. and Markwitz, A., 2012, 'Size-fractionated airborne particulate matter characterization of a residential area near Islamabad airport by IBA methods', J Radioanal Nucl Chem. 293:279–287. DOI 10.1007/s10967-012-1649-6

Wind: u and v Components. http://colaweb.gmu.edu/dev/clim301/lectures/wind/wind-uv. George Mason University. Last Modified: 2014-11-18 04:17

World Health Organization, 2013, 'IARC: Outdoor air pollution a leading environmental cause of cancer deaths', https://www.iarc.fr/en/media-centre/iarcnews/pdf/pr221_E.pdf.

World Health Organization, 2018, 'Ambient (outdoor) air quality and health', http://www.who.int/news-room/fact-sheets/detail/ambient-(outdoor)-air-quality-and-health.

Zeeshan, M. and Oanh, N. T. K., 2015, ‘Relationship of MISR Component AODs with Black Carbon and Other Ground Monitored Particulate Matter Composition’, Atmospheric Pollution Research, 62-69.

Zeeshan, M. and Oanh, N.T. K., 2014, ‘Assessment of The Relationship Between Satellite AOD and Ground PM_{10} Measurement Data Considering Synoptic Meteorological Patterns and Lidar Data’, Science of the Total Environment, 473–474: 609–618